ORE SORTING USING MICROWAVE RESONANT CAVITIES

Kelvin G. Radebe

BSc (Fort Hare), BSc(Eng) (Cape Town)

Thesis submitted to the Faculty of Engineering at the University of Cape Town in partial fulfilment of the degree of Master of Science in Electrical and Electronic Engineering.

Cape Town, April 1991

DECLARATION

I declare that this dissertation is my own unaided work. It is being submitted in partial fulfilment of the requirements for the degree of Master of Science in Engineering at the University of Cape Town. It has not been submitted before for any degree or examination at this or any other University.

K.G.RADEBE

Signature Removed

(Signature of Candidate)

25th of September, 1991

SYNOPSIS

On-line measurements of microwave properties of different materials is not new. Machines to perform these measurements have been built and commisioned in different industries, including the mining industry.

At the Premier Diamond Mine, one of the De Beers Consolidated mines situated near Pretoria in the Transvaal, separation of diamond-bearing kimberlite rock from non-diamond bearing gabbro was required. Equipment, which would be part of a large plant was required and had to be developed. This equipment would make use of the different microwave properties of the two rock types to distinguish between them and sort them into separate sections.

Initial work conducted in the Department of Electrical and Electronic Engineering at the University of Cape Town led to the development of a technique using microwave irradiation. Problems were experienced, however, with this equipment's accuracy when sorting irregularly-shaped rocks.

The objectives of this research project were to study and report on the rocks' behaviour as dielectric materials and to develop a new sorting technique with better accuracy and suitable for industrial application. Resonant cavity techniques are considered using structures such as: stripline-type structures, loop-gap resonators and split waveguide resonant cavities.

The method using split waveguide resonant cavities was finally chosen for its superior performance. The effects of the rocks and a conveyor belt running between the two parts of the split cavity were predicted. Both static and dynamic tests were then performed and the actual effects noted. Results from these tests showed that the split

cavities exhibit 100% separation between the two rock types in the absence of the conveyor belt. However, when the conveyor belt material is inserted between the two halves of the cavity, the performance is drastically degraded. In static tests, the accuracy of separation dropped to 58%. In dynamic tests, the conveyor belt attenuates the microwave signal such that no signal is observed on the receiver end.

It was then recommended that different conveyor belt material that is less attenuative to microwave signals be developed. Also, electronic circuitry to measure the Q-factor of the resonant cavity more accurately should be developed.

ACKNOWLEDGEMENTS

I wish to express gratitude to the following people for their kind assistance during this project:

- Professor B. J. Downing for his patience, guidance and support.
- the De Beers Reasearch Laboratory personnel and in particular, Dr J. D. Salter for technical assistance.
- the Foundation for Research and Development of the CSIR for their financial support.
- my special friend, Lusanda Qangule for her moral support and understanding.
- my colleagues in the Department of Electrical Engineering at UCT, namely, P. Alberts, M. Booi, S. Celliers, S. Mercer, G.Pendock and G. Rix for a lot of thought-provoking discussions.
- Mrs J. Fold for her typing services.

TABLE OF CONTENTS **Page**

LIST OF ILLUSTRATIONS

Figures **Page**

Tables **Page**

1. INTRODUCTION

In 1902, diamonds were discovered at Premier Diamond Mine near Pretoria (1). Today this mine is one of the largest and most productive mines, producing approximately 3 million carats of diamonds per year. It was at this mine where the largest natural diamond, the Cullinan, was found in 1905 (2).

Since its inception, open-cast mining techniques were employed. Several years ago, a problem arose when workings approached a thick sill of barren rock, called gabbro. The gabbro had intruded the full extent of the kimberlite pipe as shown in figure 1.1 below.

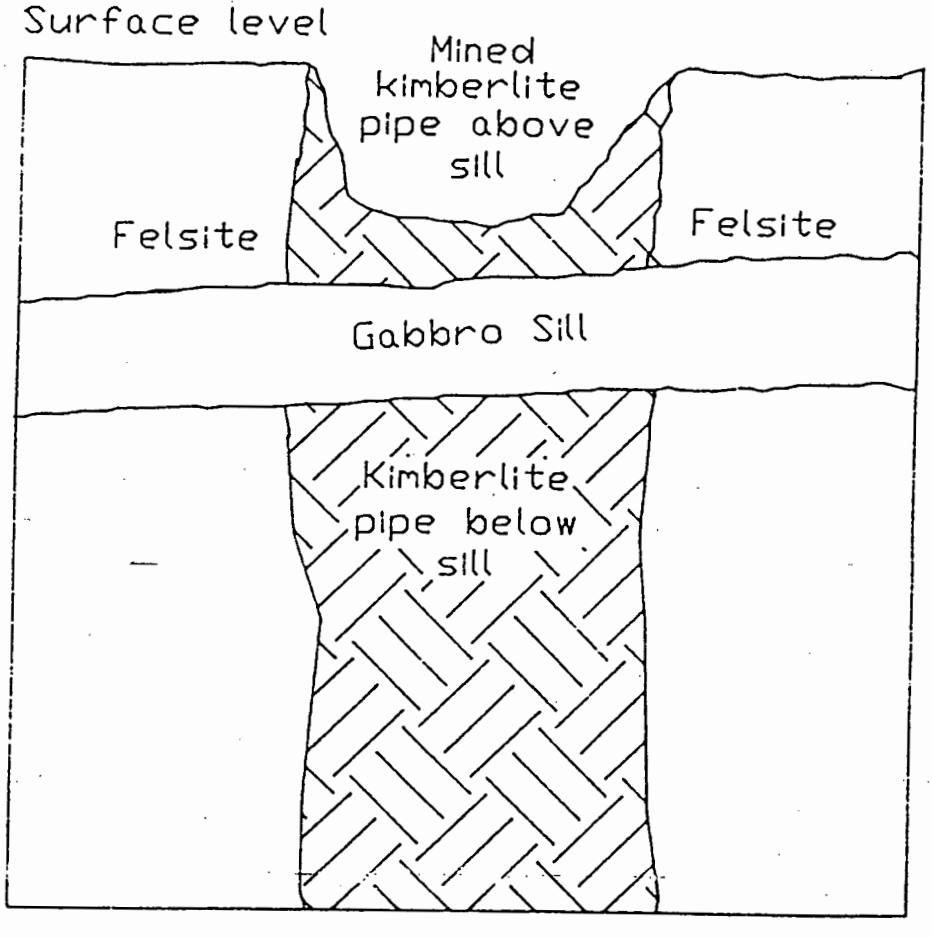

Fig 1.1 Simplified diagram of the Premier kimberlite pipe

This sill is about 75m thick and is situated approximately 400m below the surface. Due to the Premier mines' engineers' ingenuity, mining is now taking place both above and below this sill. However large volumes of gabbro fall into the mining area and contaminate the diamondiferous kimberlite. This leads to the following problems :

- the gabbro reduces the revenue-earning capacity of the treatment plant because it replaces the kimberlite.
- the gabbro increases the rate of machine wear since it is much more abrasive than the kimberlite.
- the gabbro tends to follow the diamond route through the treatment plant because of its specific gravity (3).

These factors lead to poor plant economics. Thus the need to separate the gabbro from the kimberlite is clearly seen. However, no technique of doing this was available.

Research carried out by personnel at the De Beers Research Laboratory's Mineral Processing Division and in the University of Cape Town's Department of Electrical and Electronic Engineering showed that:

- kimberlite attenuates microwave signals more than gabbro.
- kimberlite has a higher dielectric constant than gabbro.

A microwave irradiation system utilising these properties was developed to separate the different rock types. This measured the attenuation when the rock samples are passed between a microwave transmitter and a receiver. This yielded less than 100% separation between different irregularly shaped rocks (3). This was attributed to reflection of part of the signal off the rock surface.

Another system using waveguide resonant cavities was developed. This yielded 100% separation between the two rock types. However, a problem of introducing rock

samples into the cavity in industrial applications was encountered. Therefore, a new system which was mechanically suitable for industrial application and having better accuracy than the irradiation method was required. This thesis aims to report on the work done towards that end.

Some of the information on which this thesis is based was obtained from text-books and other publications in microwave engineering theory, mineralogy, electronics and rubber conveyor belts. Past theses in rock sorting using microwaves were also extensively used in this regard.

The order of presentation of the report contents is given in the next paragraph.

Chapter 2 begins by discussing general dielectric materials and their properties and in particular, how rocks behave as dielectrics. Chapter 3 then discusses microwave resonant cavities and some of their important properties. The next chapter goes on to discuss different sorting techniques that were considered. Split resonant cavities and the configurations used for static and dynamic tests are then discussed. Chapter 5 and 6 present the results and their analysis for static and dynamic tests respectively. Concluding remarks and recommendations are given in chapter 7.

2. DIELECTRIC MATERIALS AND THEIR PROPERTIES

2.1. Introduction to dielectric materials

In this chapter, dielectric materials will be discussed. Their electrical and some magnetic properties will be discussed. This is important because it will lead to understanding the effects rocks have on the microwave fields since they are also non-ferromagnetic and act as dielectrics (4).

2.2. Polarisation in dielectrics

The distribution of electric and magnetic fields inside materials may be explained by distortion of atoms inside the material or polarization (5,6). Four different kinds of polarization have been identified. These are electronic, ionic, orientation and space charge polarization. These will be discussed in turn below. The frequency dependence of polarization will also be discussed.

2.2.1. Electronic polarization

This is the type of polarization that is prevalent in all dielectrics (7). It is due to the displacement of the negative electron cloud of each atom from its positive nucleus. When an electric field **E** is applied to a dielectric, the negatively charged electrons in the individual atoms are displaced slightly in the opposite direction to **E**, relative to the heavier nuclei. This is shown schematically in figure 2.1 below.

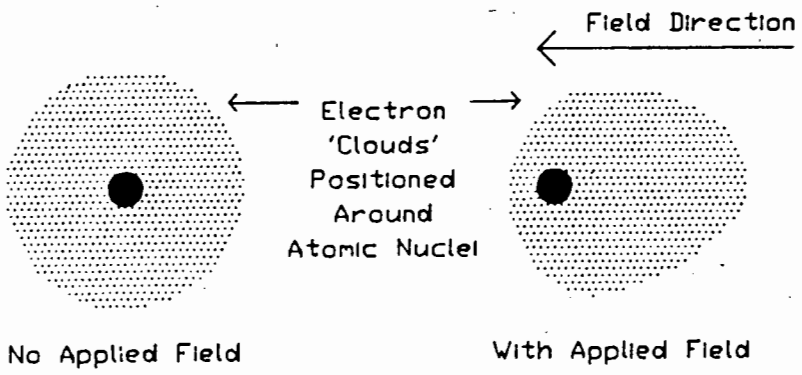

Fig 2.1 Electronic polarization

Each atom acquires an induced dipole moment of average value p_e. This is related to the electronic polarizability, denoted α_e, by the equation below:

$$p_e = \alpha_e E \qquad 2.1$$

where **E** is the ideal electric field intensity.

The magnitude of the electronic polarizability, α_e can be obtained from the properties of the hydrogen atom (8). Calculations show that:

$$\alpha_e \propto \alpha_0^3 \qquad 2.2$$

where a_0 is the radius of the first Bohr orbit and is equal to 0.53×10^{-10}m. Therefore:

$$\alpha_e = 1.5 \times 10^{-31} m^3$$

2.2.2. Ionic polarization

This is due to the displacement of adjacent ions of opposite sign (9). It is only found in ionic substances. On application of an electric field, the electronic shells deform and the ions are displaced to new equilibrium positions. This is shown schematically in

figure 2.2 below.

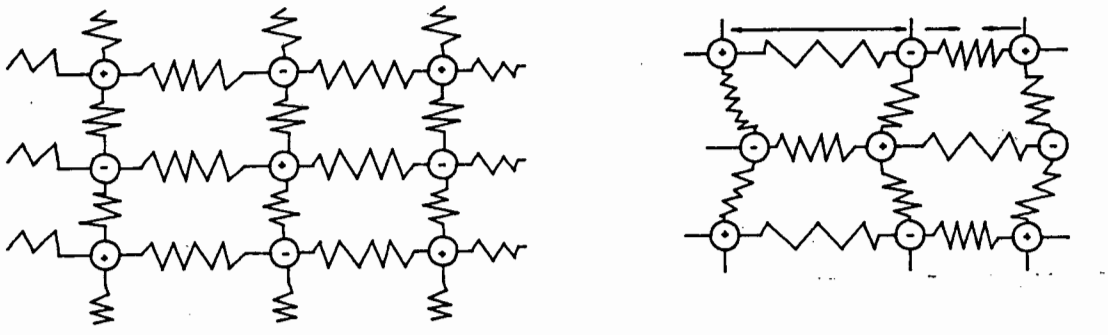

(a) No field (b) with field

Fig 2.2 Ionic polarization

It is seen in figure 2.2 above that the field distorts the lattice. Although many attempts have been made to calculate the ionic polarization, these have not been too successful. It has been determined however that this kind of polarization accounts for a very small portion of the total polarization.

2.2.3. Orientation polarization

This occurs in liquids and solids which have asymmetric molecules whose permanent dipole moments can be aligned by the electric field. This is analogous to magnetic moments which are aligned by a magnetic field. For this type of polarization to occur, the interaction energy between dipoles must be small. This is shown schematically in figure 2.3 below.

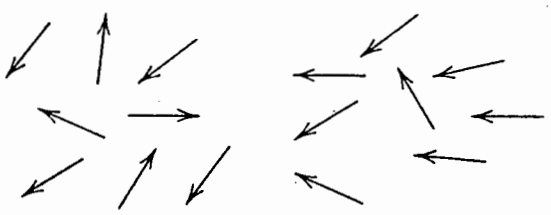

(a) No field (b) With field

Fig 2.3 Orientation polarization

As can be seen from figure 2.3 above the application of an electric field causes the permanent moments to line up in the direction of the field. However, thermal agitation tends to keep the distribution random. The result of these two opposing influences is a statistical equilibrium which permits the sample as a whole to have a dipole moment.

The orientation polarizability is then given by:

$$\alpha_0 = \frac{\mu_e^2}{3kT} \qquad 2.3$$

where μ_e = permanent moment

k = Boltzmann's constant

T = absolute temperature

At room temperature, α_0 is of the order of $10^{-23}m^3$ (10).

2.2.4. Space charge polarization

This is due to the accumulation of charges at phase interfaces in multiphase dielectrics. This type of polarization is also called interfacial polarization. It is only possible when one of the phases present in a dielectric material has a much higher resistivity than the others. Such materials are sometimes called heterogeneous. When an electrical field E is applied, some charge carriers migrate since the resistivities of dielectrics are never infinite. These migrating charge carriers are trapped at the higher resistivity phases. This sets up space charges at the interfaces and gives rise to an electric dipole moment. When averaged over all the molecules, this is equivalent to a space charge polarizability, α_s. This is shown schematically in figure 2.4 below.

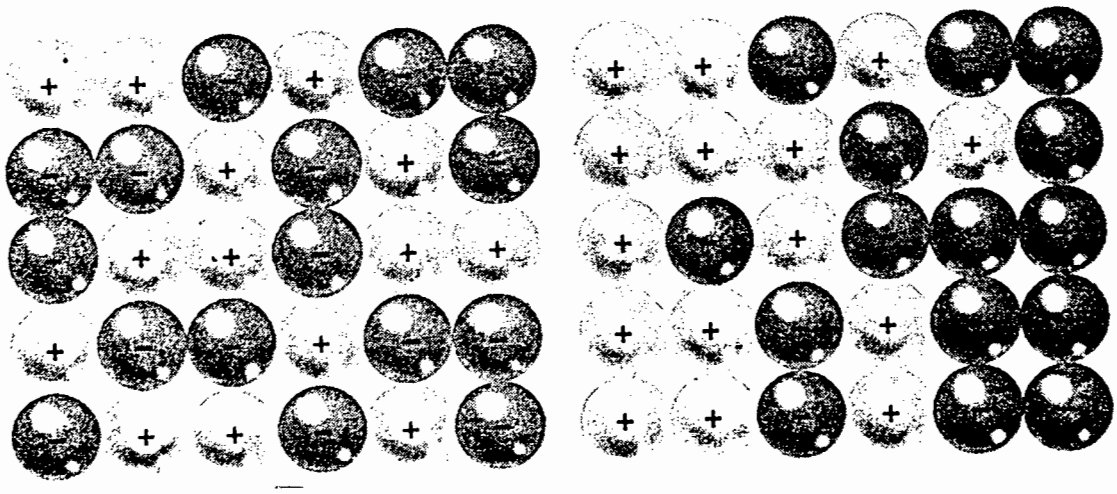

(a) No field (b) With field

Fig 2.4 Space charge polarization.

2.2.5. Frequency dependence of polarization.

The total polarizability, α is given by:

$$\alpha = \alpha_e + \alpha_i + \alpha_o + \alpha_s \qquad 2.4$$

Each type of polarization is characterized by a relaxation time t. This is the time taken for the polarization to respond to the applied field. The reciprocal of this relaxation time is the relaxation frequency. Since the relaxation frequencies of all four polarization processes differ, it is possible to separate the different combinations. The result is shown in figure 2.5 below.

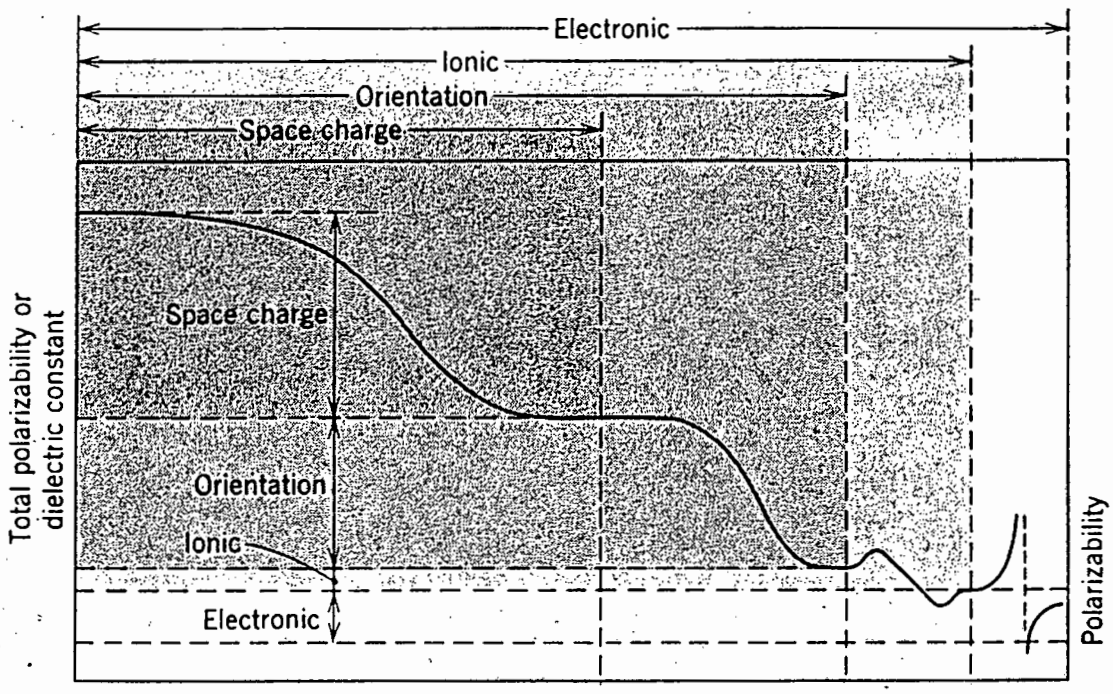

Fig 2.5 Variation of the total polarizability with frequency.

This shows four frequency ranges over which the separate polarization mechanisms operate. Generally $f_e > f_i > f_o > f_s$. When an electric field of frequency f is applied to

the dielectric material, each type of polarization can only make its full contribution provided f is less than the relaxation frequency. Since we are only interested in the microwave region, we will only consider polarization due to ionic and electronic effects.

2.3. Energy loss in dielectrics

Two mechanisms of loss of power in dielectric materials exist. One is loss due to dipole relaxation and the other is due to d c conductivity. To understand loss due to dipole relaxation we have to look at the behaviour of the materials from a macroscopic point of view. In this view we can describe what are called the constitutive parameters of the material. These are the permittivity ϵ and the permeability μ. The electric flux density **D** is broken into two parts. The first relates it to the electric field by the free-space permittivity ϵ_0. The second is called the polarization **P**. That is:

$$\mathbf{D} = \epsilon_0 \mathbf{E} + \mathbf{P} \qquad 2.5$$

Similarly, the magnetic flux density can be written:

$$\mathbf{B} = \mu_0(\mathbf{H} + \mathbf{M}) \qquad 2.6$$

where **H** is the magnetic field intensity and **M** is the magnetic polarization; commonly called the magnetization.

For linear materials **P** is directly proportional to **E**. The constant of proportionality is $\epsilon_0 \chi_e$. This leads to the following relation:

$$\mathbf{P} = \epsilon_0 \chi_e \mathbf{E} \qquad 2.7$$

where χ_e is called the electric susceptibility.

The permittivity ϵ_0 is related to χ_e by:

$$\epsilon = \epsilon_0(1 + \chi_e)$$

2.3.1. Loss due to dipole relaxation

The classical development of the relations between this dielectric constant, loss and frequency is due to Debye. A periodic electric field is assumed. i.e:

$$\mathbf{E} = E_0 \cos \omega t \qquad 2.8$$

where E_0 is independent of time t and ω is the frequency.

Equation 2.8 can be rewritten as:

$$\mathbf{E} = E_0 e^{i\omega t}$$

This leads to **D** also being periodic. **D** is normally out of phase with **E** with ø as the phase shift. i.e.

$$D = D_0 \cos(\omega t - \phi) = D_1 \cos \omega t + D_2 \sin \omega t$$

where

$$D_1 = D_0 \cos \phi, \quad D_2 = D_0 \sin \phi \qquad 2.9$$

Two different dielectric constants may be written:

$$\epsilon' = \frac{D_1}{E_0}$$

and

$$\epsilon'' = \frac{D_2}{E_0}$$

From Equation 2.9,

$$\frac{\epsilon''}{\epsilon'} = \tan\phi$$

This is the expression for the loss tangent.

2.3.2. Loss due to d c conductivity

There usually exists charge carriers that can move about inside a dielectric subjected to high electric fields. This leads to a non-zero conductivity and to normal ohmic losses as found in conductors. These losses increase with decreasing frequency at low frequencies. It can easily be seen why this is so from equation 2.10 below. This equation relates conductivity σ, frequency ω, and ϵ''.

$$\sigma = \omega\epsilon'' \qquad 2.10$$

where all the parameters are real.

2.4. Rocks as dielectrics

Rocks can be thought of as multiphase systems made up of minerals with different chemical compositions (11). Most of the types of polarisation discussed earlier take place in them. This results in the dielectric permeability and energy loss being a complicated function of frequency, temperature, pressure and other factors. However a variety of equations have been used to estimate the dielectric constants of rocks (12,13,14). In these calculations, the rocks are considered as matrices or mixtures of various individual components comprising the material.

Since rocks are such complicated materials, both in composition and structure, it is not surprising to find that no simple relationship exists between their physical properties and their chemical or mineral composition. Values of the dielectric constants making up the rocks vary over two orders of magnitude. This is an adequate variability, so that one might expect some differentiation between rock types on the basis of bulk dielectric constant. This is exactly the property that is exploited to separate the two rock types i.e diamondiferous kimberlite and barren gabbro, in this project.

3. MICROWAVE RESONANT CAVITIES

At high frequencies and short wavelengths i.e. less than one metre, conventional circuit elements have dimensions comparable to the wavelengths. These circuits lose energy by radiation. Also, conventional wire circuits have high resistances because of skin effects. These two phenomena dictate that the circuit region be shielded and completely surrounded by a good conductor to prevent radiation. This results in a hollow conducting box with the electromagnetic energy confined inside (15). This is called a cavity resonator and is the topic of this chapter. The following sub-topics will be discussed in this chapter:

- Energy storage mechanism of resonant cavities.
- Power dissipation in resonant cavities.
- Resonant frequencies and Q-factor.
- Electric and magnetic fields in resonant cavities.
- Coupling energy into and out of a cavity.
- Effects of dielectric materials inside the cavity.

It will be seen from future chapters that only rectangular resonant cavities are of interest to us. Therefore discussion will be restricted to these.

3.1. Electric and magnetic fields in resonant cavities

The dominant modes in rectangular cavities are the transverse electric (TE_{101}) and the transverse magnetic (TM_{111}) modes. These are dominant because they result in the lowest resonant frequency. In this project, the TE_{101} mode was chosen for ease of coupling and reasonable physical dimensions. Discussions will be limited to this mode. A drawing of the resonant cavity and the electric field distributions for this mode are

shown in figure 3.1 below.

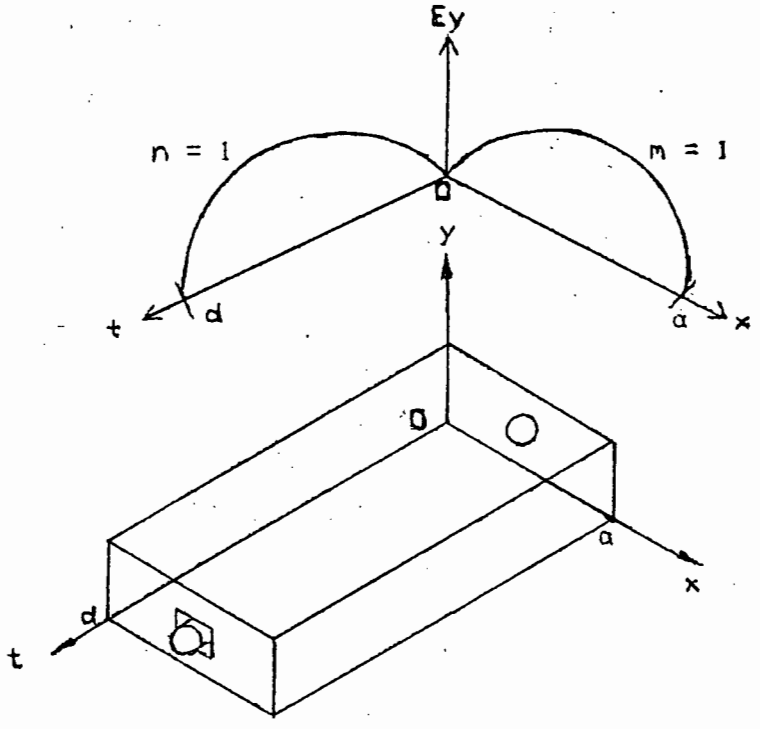

Fig 3.1 A rectangular resonant cavity and electric field distributions.

The magnetic field lines will be concentric and lie in the xz-plane as shown in figure 3.2 below.

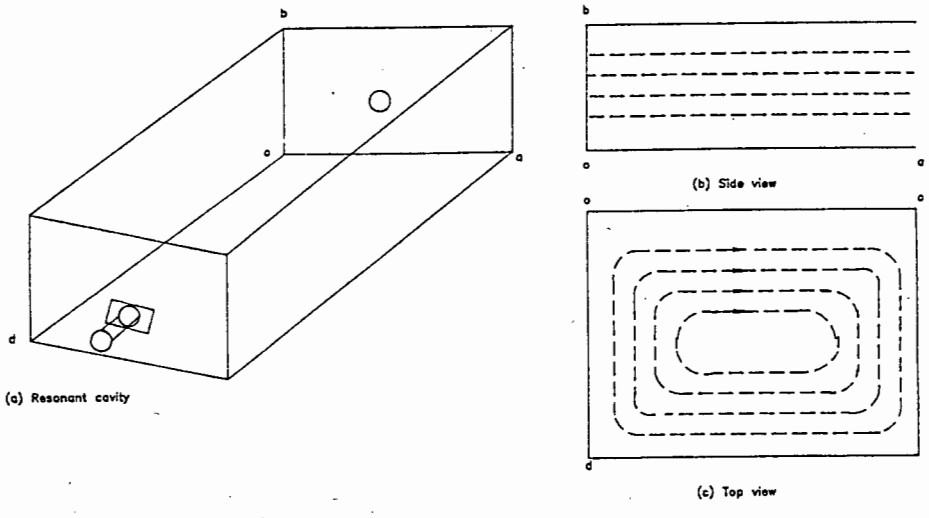

Fig 3.2 A resonant cavity and magnetic field distribution.

The next section will address the question of how power is dissipated in resonant cavities.

3.2. Power dissipation in resonant cavities

In a lossless cavity made up of perfectly conducting walls and filled with a perfect loss free dielectric, no power loss exists. The small amount of energy coupled in never decays. It just transfers back and forth between the electric and magnetic fields. However, walls have finite conductivities and dielectrics ,including air, have non-zero conductivities. This leads to fields existing inside the conducting wall. The field amplitude decays quite quickly i.e. to 1/e of its value at the inside surface in a distance δ, called the skin depth. δ is given by:

$$\delta = \sqrt{\frac{2}{\omega \mu \sigma}}$$

where μ and σ are constitutive parameters of the conductor.

In a good conductor the conductive current is much greater than the displacement current i.e. $\sigma \gg \omega\epsilon$ and the skin depth is very small at microwave frequencies.

The power lost in the conducting walls is then given by:

$$P_c = \frac{1}{2} R_s \int_{walls} |H_t| ds \qquad 3.1$$

where $R_s = 1/\delta\sigma$ is the surface resistivity of the metallic walls and H_t is the tangential magnetic field at the surface of the walls.

3.3. Resonant frequency and Q of the TE_{101} mode

To determine the resonant frequency of the TE_{101} mode requires the solution of Maxwells equation and substitution of the boundary conditions. This is done in Appendix I for a general TE_{mnl} mode. The resulting resonant frequency is given by:

$$f_{mnl} = \frac{c}{2\pi\sqrt{\mu_r \epsilon_r}} \sqrt{\left(\frac{m\pi}{a}\right)^2 + \left(\frac{n\pi}{b}\right)^2 + \left(\frac{l\pi}{d}\right)^2} \qquad 3.2$$

where c = speed of light and μ_r and ϵ_r are the relative permeability and permittivity of the material filling the cavity respectively.

For the TE_{101} mode to be dominant, b > a > d.

Letting $E_0 = -2jA^+$ in equation 12 (Appendix I) and keeping in mind that $A^- = -A^+$ the following is obtained for the TE_{101} mode:

$$E_y = E_0 \sin\frac{\pi x}{a}\sin\frac{\pi z}{d} \qquad 3.3a$$

$$H_x = \frac{-jE_0}{Z_{TE}}\sin\frac{\pi x}{a}\cos\frac{\pi z}{d} \qquad 3.3b$$

$$H_z = \frac{j\pi E_0}{k\eta a}\cos\frac{\pi x}{a}\sin\frac{\pi z}{d} \qquad 3.3c$$

where

$$Z_{TE} = \frac{E_x}{H_y} = \frac{-E_y}{H_x} = \frac{\omega\mu}{\beta} = \frac{k\eta}{\beta}$$

and

$$\eta = \sqrt{\frac{\mu}{\epsilon}}$$

is the intrinsic impedance of the material filling the wave guide. This clearly shows that the fields form standing waves inside the cavity.

In order to determine the Q, the stored electric and magnetic energies and the power lost in the conducting walls and the dielectric have to be computed. To calculate the power lost, equation 3.3b and 3.3c are substituted into equation 3.1 to give:

$$P_c = \frac{1}{2}R_s\left\{2\int_{y=0}^{b}\int_{x=0}^{a}|H_x(z=0)|^2dxdy + 2\int_{z=0}^{d}\int_{y=0}^{b}|H_z(x=0)|^2dydz + 2\int_{z=0}^{d}\int_{x=0}^{a}|H_x(y=0)|^2 + |H_z(y=0)|^2dxdz\right\}$$

$$\therefore \quad P_c = \frac{R_s E_0^2\lambda^2}{8\eta^2}\left(\frac{ab}{d^2} + \frac{bd}{a^2} + \frac{a}{2d} + \frac{d}{2a}\right) \qquad 3.4$$

where the symmetry of the cavity has been used in doubling the contributions of the walls at x=0, y=0 and z=0 to account for the contributions at the walls at x=a, y=b and z=d respectively.

The stored electric energy is given by:

$$W_e = \frac{\epsilon}{4}\int_v E_y E_y^* dv \qquad 3.5$$

Substituting eq 3.3a into eq 3.5 we obtain:

$$W_e = \frac{\epsilon abd}{16} E_0^2 \qquad 3.6$$

But at resonance, the stored electric energy is equal to the stored magnetic energy. Therefore $W_e = W_m$ and the total energy stored becomes:

$$W_t = 2W_e = \frac{\epsilon abd}{8} E_0^2 \qquad 3.7$$

Therefore the Q of the cavity with lossy conducting walls but lossless dielectric is:

$$Q_c = \frac{\omega W_T}{P_c} = \frac{(kad)^3 b\eta}{2\pi^2 R_s} \frac{1}{2a^3b + 2bd^3 + a^3d + ad^3} \qquad 3.8$$

3.4. Effects of dielectric materials inside the cavity

The previous analyses assumed that the cavity was filled with air which acts as a good dielectric. However, if the cavity were to be filled with a lossy dielectric of complex permittivity $\epsilon = \epsilon' - j\epsilon''$, conductivity σ and permeability μ; then more power would be dissipated in the dielectric. The extra power dissipated is given by:

$$P_d = \frac{1}{2}\int_v \mathbf{J}\mathbf{E}^* dv = \frac{1}{2}\omega\epsilon''\int_v |\mathbf{E}|^2 dv \qquad 3.9$$

where $\mathbf{J} = \mathbf{J}_s + \sigma\mathbf{E}$ is the total electric current density

$\mathbf{J}_s$ is the electric source current density

$\sigma\mathbf{E}$ is the current density arising from the conduction current.

Substituting **E** from equation 3.3a into equation 3.9, the following is obtained:

$$P_d = \frac{abd\omega\epsilon''}{8}|E_0|^2 \qquad 3.10$$

Therefore the Q of a cavity with a lossy dielectric and perfectly conducting walls is:

$$Q_d = \frac{2\omega W_e}{P_d} = \frac{\epsilon'}{\epsilon''} = \frac{1}{\tan\delta} \qquad 3.11$$

where tan δ is the loss tangent.

When both wall losses and dielectric losses are present, the total power loss is P_c + P_d and the total Q becomes:

$$Q = \left(\frac{1}{Q_c} + \frac{1}{Q_d}\right)^{-1} \qquad 3.12$$

This shows that loading the cavity with any material of dielectric constant higher than that for air reduces the cavity Q. It is obvious that the higher the dielectric permittivity, the lower the Q-value. Further, the greatest effect on the Q occurs if the dielectric is in a position of maximum electric field. For a rectangular cavity operating in TE_{101} mode this is at the centre.

A useful relation that is often used to estimate the Q of a resonant cavity is:

$$Q \approx \frac{f_0}{\Delta f} \qquad 3.13$$

where f_0 is the resonance frequency and Δf is the bandwidth.

The bandwidth is taken as the frequency range between the two halfpower points.

Although rectangular resonant cavities can yield Q-values in the order of 10,000 such high Q-values are only obtained from silver plated cavities with only a small amount of power coupled to the output load. Disturbances caused by the coupling system, surface irregularities, dielectric losses, radiation from small holes and other perturbations increase the losses and thus decrease the Q. Some of these effects are discussed more extensively in the next chapter which deals with resonant cavities that have been divided into two parts.

3.5. Coupling energy into and out of a resonant cavity

Different methods of coupling the cavity to external circuitry exist. It is possisble to couple onto the E-field or onto the H-field. Methods of coupling include:

- iris coupling
- magnetic loop coupling
- E-field probe coupling

These will briefly be described below. A more thorough discussion can be found in (16).

3.5.1. Iris coupling

In this form of coupling, the field components of electric and magnetic field lines are as shown in figure 3.3(a) and (b) below:

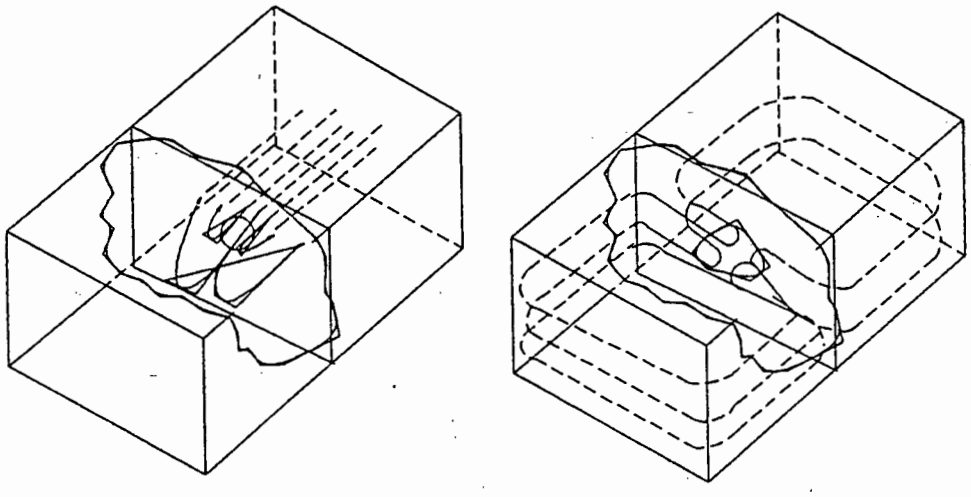

(a) (b)

Fig 3.3 Electric and magnetic field lines in iris coupling

3.5.2. Loop coupling

A conducting loop with its plane normal to the magnetic field lines is introduced into the cavity. The circular H-field around the conductor couples to the H-field of the cavity. This is shown in figure 3.4 below:

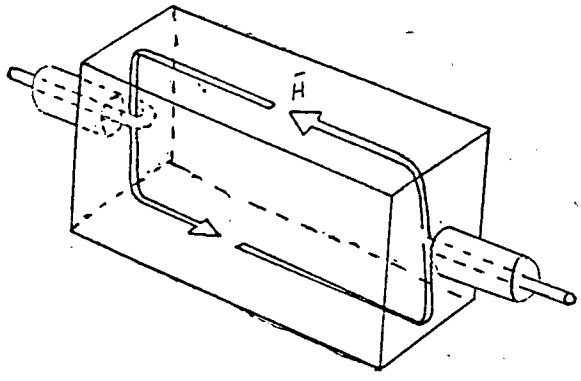

Fig 3.4 Magnetic field lines in loop coupling

3.5.3. E-Field probe coupling

A short conducting probe is introduced into the cavity in the direction of the electric field lines. The probe must be thin and of uniform thickness. The physical arrangement is shown below.

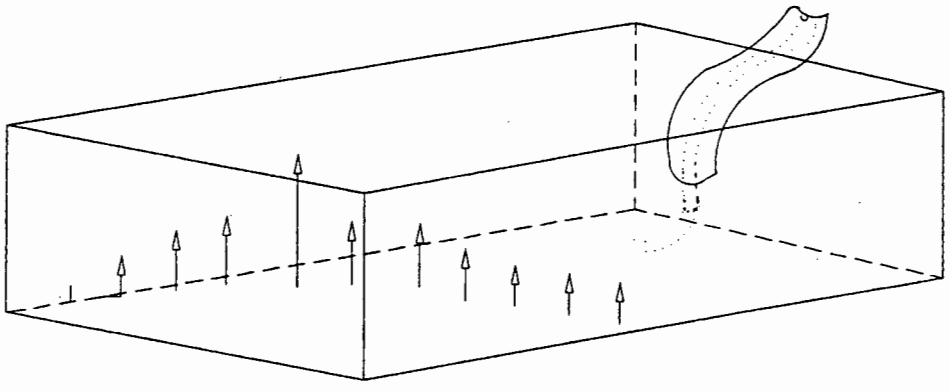

Fig 3.5 Electric field lines in probe coupling.

The theory discussed above has been shown to be very accurate (17). However, some factors arising from necessary practical implementation will cause deviation from it. Practical implementation of a rectangular cavity is discussed in the next chapter.

4. EXPERIMENTAL TECHNIQUES

Many experiments to measure dielectric constants of different materials have been performed (18-33). In this project, however, absolute measurement of permittivity was not required. It was required to sort the two different rock types using the properties of different complex dielectric constants. In this chapter, a few of the methods that were considered are discussed. The method that was finally chosen, together with a description of the equipment used is also discussed.

4.1. Some sorting techniques

Microwave sorting techniques can be divided into two types; open structures and closed structures. They are discussed in the subsections below together with the disadvantages of each.

4.1.1. Microwave irradiation

In this technique, the rocks are individually irradiated with microwaves via a transmitting antenna as shown in figure 4.1. A receiving antenna connected to a detector is placed on the opposite side of the rock. The attenuated microwave signals are then received on the receiver end. A rock can then be identified based on how much the transmitted signal was attenuated.

Horn anntenas were used on both the transmitter and the receiver side. The rock samples are fed through the system on a conveyor belt. Figure 4.1 shows the system configuration. The operation of the different parts is controlled by electronic hardware and a microcomputer.

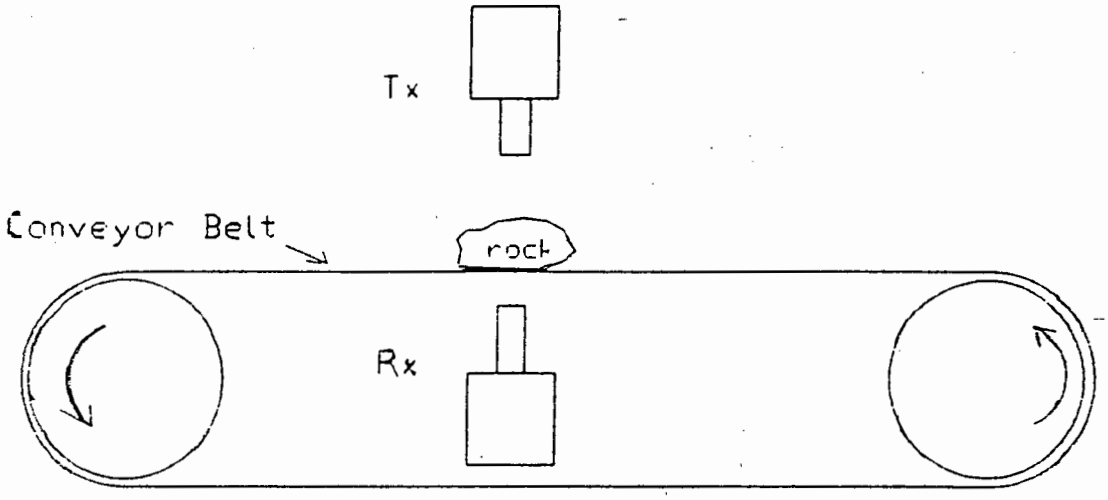

Fig. 4.1 Physical configuration of microwave irradiation method.

When a rock sample has been identified as kimberlite, it is allowed to fall freely onto another conveyor belt for transportation to the crusher. However, if it is identified as a gabbro sample, a jet of air deflects it onto another conveyor belt for transportation to a waste rock pile.

4.1.2. Resonant cavity techniques

In this technique, a "closed" waveguide resonant cavity is used. A closed waveguide was chosen for its high Q-factor which leads to high sensitivity and makes detection possible for small changes in the complex dielectric constant of the material inside the cavity. This occurs when a rock is introduced into the air-filled cavity and can be described by the expressions for Q_c and Q_d as given in equations 3.8 and 3.11 respectively.

The resonant frequency was found to change when the rocks were introduced into the cavity. However, the change in frequency was inconsistent over many rock samples and

could not be used reliably to sort the two rock types. Therefore its determination was not pursued. The mechanism causing this inconsistency was due to the kimberlite rock being inhomogeneous and an-isotropic. The propagation velocity of the microwave signal thus varies with sample orientation giving an apparent variation of relative permittivity with rock sample orientiation.

The resonant frequency of the cavity was chosen to be about 500MHz which resulted in a cavity of suitable physical dimensions. This resonant frequency led to the following dimensions for the resonant cavity.

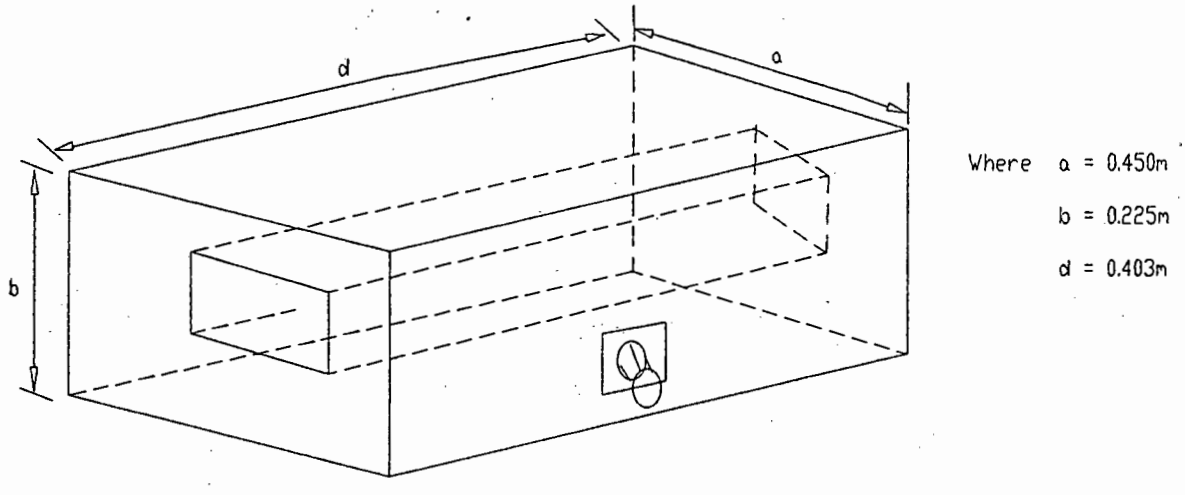

Fig 4.2 Resonant cavity dimensions

Figure 4.2 above also shows the slots cut on opposite sides of the cavity to feed the rocks through the cavity. A discussion on the choice of the two sides on which to cut the slots is presented in Appendix II. The determination of the cavity dimensions is also shown in Appendix II.

Figure 4.3 below shows the physical configuration for this technique.

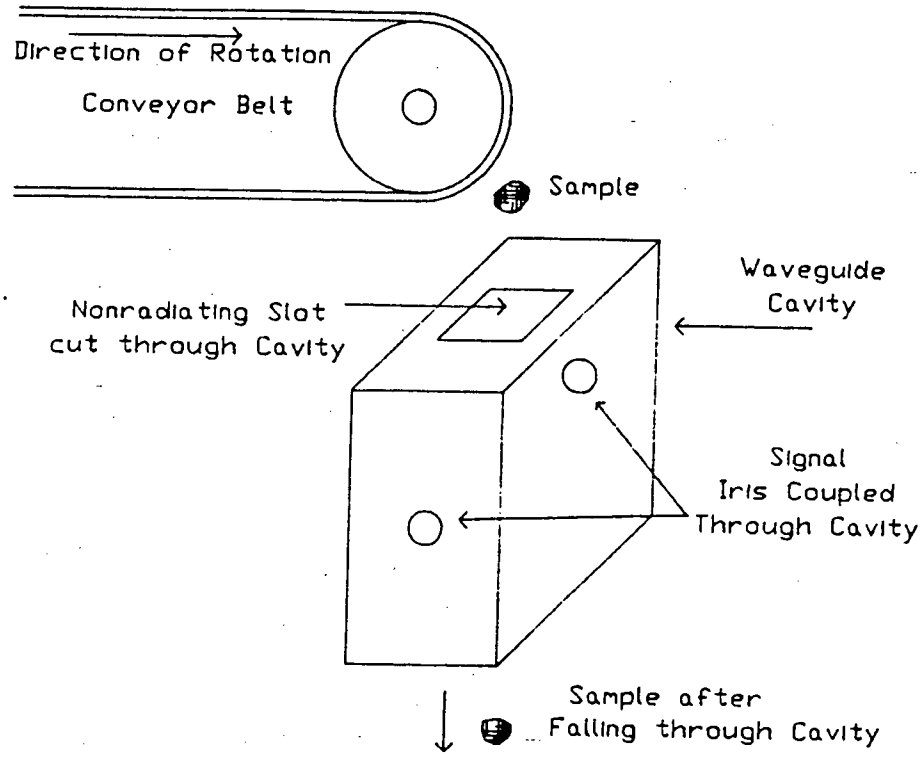

Fig 4.3 Physical configuration of resonant cavity technique.

As before, a rock sample ends up at a different destination depending on what type it is.

4.1.3. Disadvantages of these techniques

Both of these techniques are viable for ore sorting. However, there are some problems with their operation. These will be discussed first for the irradiation method and then for the resonant cavity method.

(a) Problems with the irradiation method

The major problem with the irradiation method was its inaccuracy. In a system that was developed in the Department of Electrical and Electronic Engineering at the University of Cape Town, this method yielded only 49% gabbro rejection for a 94.5% kimberlite recovery in dynamic tests (34).

This was shown to have been caused by reflection of the microwave signal from the irregular shaped rocks.

Other problems were caused by multi-path propagation and adjacent channel interference described by Booi (35).

(b) Problems with the resonant cavity technique

The problems described above do not occur in a closed cavity system (36-38). Although this method gave 100% separation of gabbro from kimberlite, a problem exists with feeding rocks through the cavity. The proposed system of allowing rocks to fall through the cavity in free fall was discarded as not being viable. This was due to the variation in trajectory of rocks ejected from the end of the conveyor belt shown in figure 4.3 and thus the prospect of a finite percentage of ejected rocks failing to enter the hole in the cavity. A tapered funnel to guide the rocks ejected from the end of the conveyor belt was rejected due to the possibility of a rock being jammed in the funnel. Previous experience in the mining environment has shown that guiding funnels were not viable.

We were therefore left with two systems each of which had strong and weak points. The ideal system would be to combine the strong points of both methods. It should

have the accuracy of the resonant cavity technique coupled with the superior rock feeding mechanism of the irradiation technique. Several techniques with improved rock presentation were considered and are discussed in the section below.

4.2. Alternative Sorting Techniques

A number of different methods of sorting were considered. In all these methods appreciable differences in behaviour were required for loads of differing dielectric constants. It was also required that these techniques be capable of being used on-line i.e. they should be able to sort samples travelling on a moving conveyor belt. In order to ease the material presentation problem open resonant structures were investigated. The structures considered are microstrip, parallel stripline, shielded stripline, coplanar stripline and loop-gap resonators. A discussion of these follows. Due to their similarity the stripline-type structures will be discussed together, followed by a discussion of loop-gap resonators.

4.2.1. Stripline-type structures

In these structures, a strip conductor and a ground plane are separated by a dielectric material (39-42). In our case, air is used as the dielectric. The electric and magnetic field lines are not entirely contained in the dielectric substrate. Therefore the wave propagation in the microstrip line is not a pure transverse electromagnetic mode (TEM) but a quasi-TEM mode (39).

The stripline-type structures are differentiated according to the dimensions and position of the strip conductor with respect to the ground plane. Diagrams showing these structures and their field patterns are given in figures 4.4-4.7 below (43).

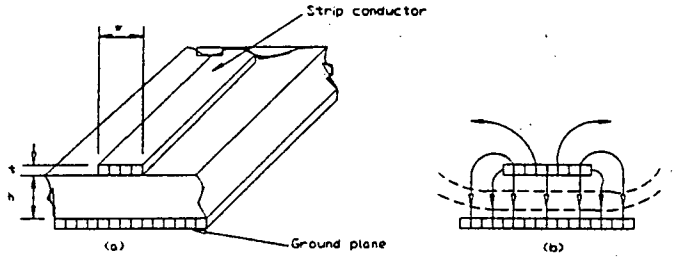

Fig 4.4 Microstrip

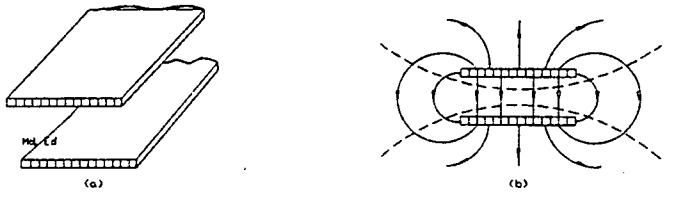

Fig 4.5 Parallel Stripline

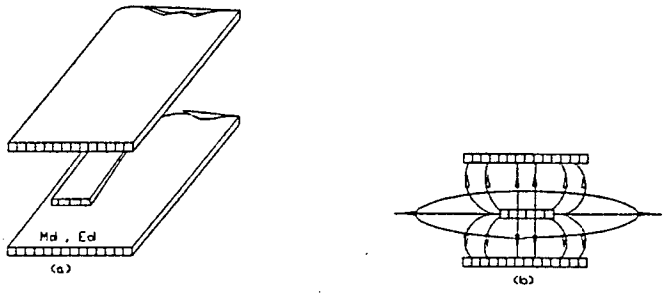

Fig 4.6 Shielded Stripline

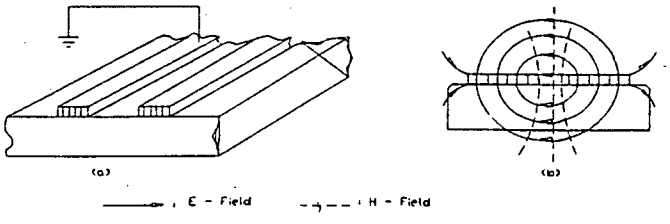

Fig 4.7 Co-planar Stripline

The diagrams above show that in all these structures, radiation into space occurs. This is worst in the case of microstrip and better for shielded stripline. Although these

structures are open and ore samples can be passed through a resonant cavity using these structures on a conveyor belt, they were found unsuitable for discriminating between the rock types. This was thought to arise from:

- low field concentration inside the structure.
- low quality factors compared to a closed waveguide.
- reflected signals are not confined in the cavity and radiate into free space.

These observations led to the conclusion that partially closed structures with a high Q-factor were required. One such structure is the loop-gap resonator discussed below.

4.2.2. Loop-gap resonators (LGR)

This is a newly developed microwave resonant structure. It has a field distribution that is intermediate between lumped and distributed (44). The diagrams showing physical structure and field patterns are given in figure 4.8.

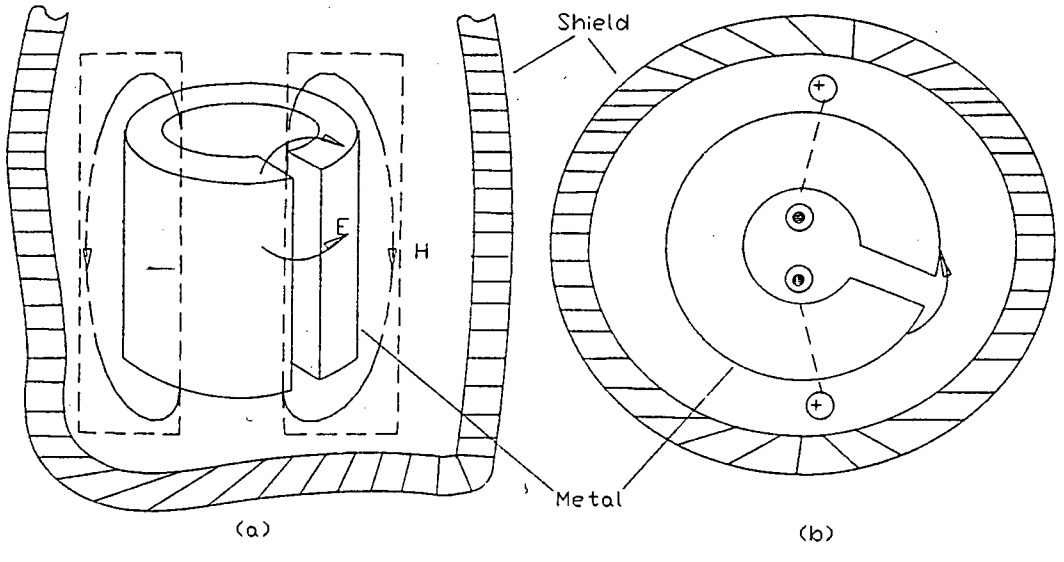

Fig 4.8 Loop gap resonator.

The LGR may be regarded as a high Q-factor parallel tuned circuit. The parallel gap is equivalent to a capacitor and the loop is the equivalent to the inductor. The LGR frequency can be tuned by altering the dielectric constant of the material filling the gap. Passing gabbro and kimberlite through the resonator close to the gap should hopefully generate sufficient change in frequency to discriminate between the two rock types.

Initial tests on a 30mm diameter with small samples showed high sensitivity to variation in dielectric constant when the sample was close to the gap. However, this sensitivity is not uniform across the resonator. This was due to the non-uniform field distribution of the LGR. For this reason the LGR was abandoned as a structure that could be used for ore sorting.

The structure required was one without the shortcomings of stripline-type structures and loop-gap resonators yet still open enough to easily feed rocks through; a structure like an "open" waveguide resonant cavity. This line of thinking led to the development of a novel new structure which we called a split resonant cavity. This structure is discussed in the next section.

4.3. Split resonant cavities

Waveguide resonant cavities are closed high Q structures (45). Our application requires that they be more "open" to introduce samples inside. These "openings" were small non-radiating slots. Using the slots, 100% separation was achieved. However, it was shown that these small slots were not practical for mechanical presentation of the rock samples. A structure that could work with a conveyor belt feed mechanism was required. This led to the use of a resonant cavity split into two parts, but coupled

together electrically. One part would then be mounted above the conveyor belt and the other below with the conveyor belt passing between the gap. This new open cavity led to a large physical discontinuity and is shown in figure 4.9 below.

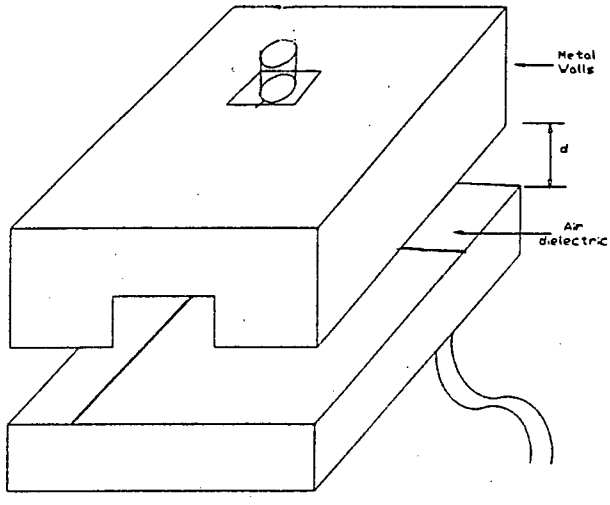

Fig 4.9 Split resonant cavity

Cutting the resonant cavity into two parts leads to characteristics that are different from those of a normal closed resonant cavity. The main effects are changes in field distributions, resonant frequency and Q-factor. These are discussed in the subsections below. To determine how this structure would perform with the samples being fed through on a conveyor belt and the effects the conveyor belt itself, a consideration of the field structure of the split cavity is presented below.

4.3.1. Field distributions in split resonant cavities.

The field analysis of most discontinuity problems is very difficult (46), and beyond the scope of this thesis. However, a basic attempt of explaining the field distributions in

this new structure will be made. Unlike the field structure in a closed cavity, the fields are no longer contained inside the cavity. Some radiation occurs out of the thin gap. This results in a distortion of the field distributions. Approximations of these are shown in figure 4.10 below. The field distributions of the entirely closed cavity is shown in figure 4.10(a). The effects of the openings in the cavity on the field structure is shown in figure 4.10(b) and the additional effects of the gap to the split cavity is shown in figure 4.10(c).

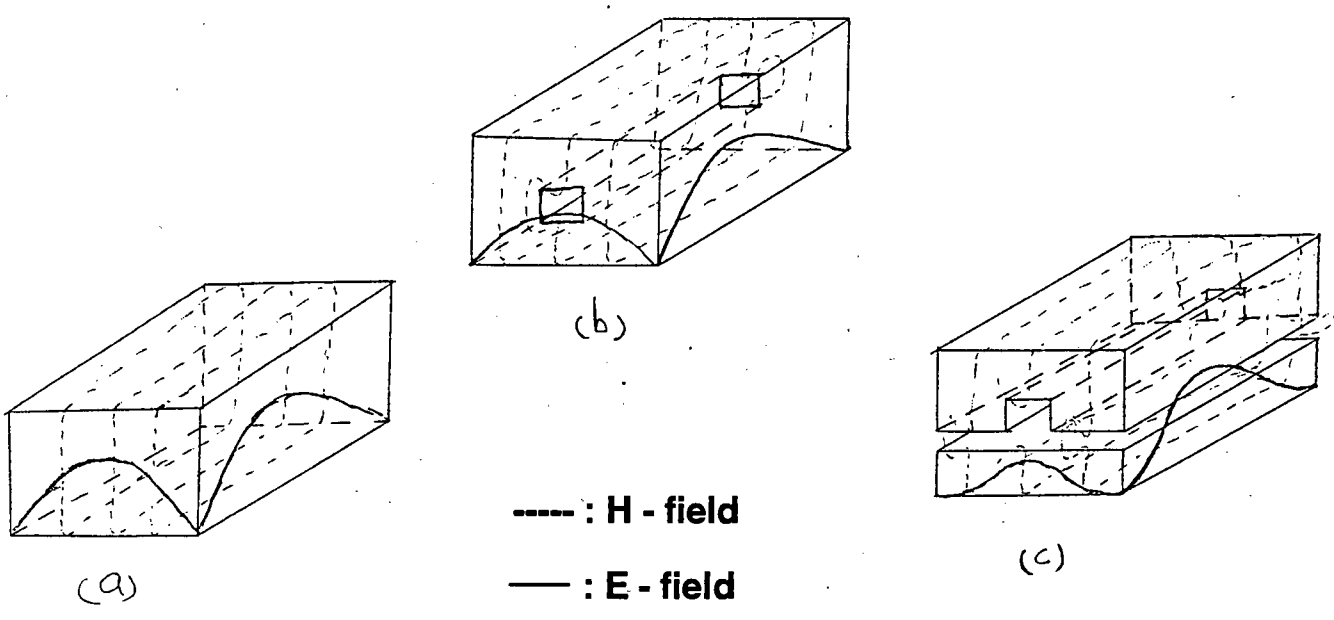

Fig 4.10 Field distributions in different cavities.

The diagram in figure 4.10(c) above shows that some of the H-field is radiated into free space while some is still contained inside the cavity but the fringing field will be external. Of more importance to us is the E-field. This is shown to go to zero before the cavity boundaries are reached leading to an effective reduction in the size of the cavity. This is because radiation exists at the boundaries.

4.3.2. Resonant frequency and Q of the cavity.

The smaller effective size of the cavity is expected to cause an increase in the resonant frequency. This can be seen from equation 3.2 which gives the expression for resonant frequency as a function of the cavity dimensions.

Equation 3.8 shows that the cavity Q-factor Q_c is inversely proportional to the surface resistance R_s of the metal. For a good conductor R_s is given by Pozar (47) as:

$$R_s = \frac{1}{\sigma \delta_s} = \sqrt{\frac{\omega \mu}{2\sigma}}$$

where σ = conductivity of the metal

δ_s = skin depth

ω = angular frequency

μ = permeability

With a thin gap in the resonant cavity, surface currents have to travel through air which has extremely low values of conductivity. This leads to a huge reduction in the cavity Q-factor. The dielectric Q factor, Q_d, on the other hand, is not affected since the loss tangent remains that of air.

4.3.3. Predicted effects of rubber conveyor belt material on cavity.

Since the split resonant cavity is going to be used with a rubber conveyor belt, it is necessary to determine what effect it would have on the cavity characteristics.

The conveyor belt has dielectric constant and loss tangents that are different from those of air. Natural rubbers have relative dielectric constants ϵ_r around 2.4 (48). This

figure is slightly higher for rubber mixed with other materials as is the case in the manufacture of conveyor belts. To improve the wear properties, conveyor belts are usually made of india-rubber and specially woven cotton duck. Each ply of the cotton duck is stretched and then impregnated with rubber. The finished belt is then coated on both sides with rubber and then vulcanised under pressure. This vulcanisation leads to an increase of about 1.5% in in dielectric constant from 2.40 to 2.43. The bigger increase however is in the loss tangent which increases by about 260% from 0.005 to 0.018 at 100MHz (48,50). It is to be noted that these increases are lower at lower frequencies.

Equation 3.2 shows the resonant frequency is proportional to $\sqrt{\epsilon_r}$. The resonant frequency for the cavity loaded with the conveyor belt will therefore be slightly reduced. A more pronounced change is expected in Q_d due to the large increase in the loss tangent. This will lead to Q_d dominating the system Q; leading to its overall decrease.

In order for all the effects predicted in the previous sections to be measured, equipment was set up. Measurements were taken for both static and dynamic tests. These refer to when samples are stationary inside the cavity and when they are passing through the cavity respectively. These equipment configurations are discussed in the following two sections.

4.4. Configuration for static tests

Measurements of the resonant frequency and Q of the empty cavity were required. The cavity was then loaded with either kimberlite or gabbro and these parameters were measured. Even though in the final application these measurements were to be done on moving samples, the initial tests were done on stationary rocks.

The equipment used to do these measurements consisted of:

- a split resonant cavity as discussed in the previous section.
- an HP8359SA RF plug in source.
- an HP8350B sweeper.
- an HP8746B S-parameter test set.
- an HP8411 converter.
- an HP8410C network analyzer.
- an HP8412B phase magnitude display.

A schematic diagram of the equipment configuration is given in figure 4.11 below.

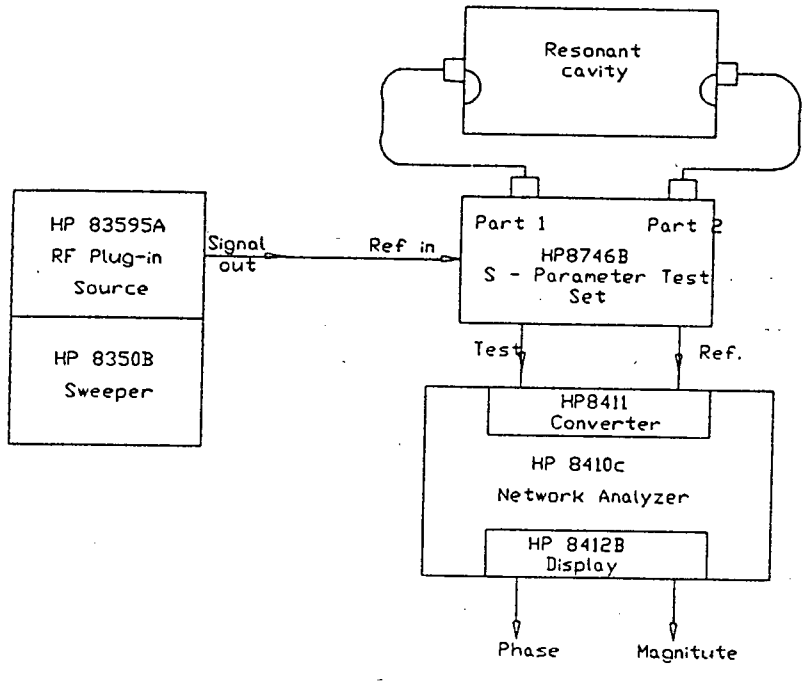

Fig 4.11 Measurement system for the static case.

A brief description of the measurement system and its operation is given below.

The microwave signal is fed to the S-parameter test set. This signal is swept in frequency from 450MHz to 550MHz to ensure the cavity resonance. This cavity is connected across the two ports of the S-parameter test set. The transmission coefficient S_{21} is measured and displayed on the phase/magntidue display of the network analyzer. The resonant frequency f_0 and the two frequencies f_1 and f_2 at which the displayed signal is 3dB below the maximum are measured manually. The difference between f_1 and f_2, $\Delta f = f_2 - f_1$ gives the half-power bandwidth. Equation 3.13 is then used to approximate the unloaded Q of the resonant cavity under test. Rock samples are then introduced into the cavity and the new Q values determined. These rocks are supported in the cavity centre by thin strips of polystyrene material. Polystyrene was chosen because of its low relative dielectric constant and low loss tangent. For this reason, it is quite transparent to microwave signals at the frequencies of interest.

The Q values for the unloaded cavity, for the cavity loaded with gabbro and for the cavity loaded with kimberlite were compared. According to the theory discussed in section 2.4, the Q for the unloaded cavity was expected to be highest and that for the cavity loaded with kimberlite lowest.

After the system was found to work satisfactorily for stationary rocks, measurements were taken for moving rocks. The rocks were required to move at 5m/s; the speed at which they will be moving on the conveyor belt used in the final application.
The equipment used for taking dynamic measurements consisted of:

- a split resonant cavity (as before)
- a conveyor belt simulator
- electronic circuitry
- IBM PC.

Each of these, except for the split resonant cavity, is discussed in the subsections below.

4.5. Configuration for dynamic tests

4.5.1. Conveyor-belt simulation

Rocks were dropped in free fall and guided through a vertical hollow metallic cylindrical pipe to simulate a conveyor belt moving at 5m/s. Its length is chosen such that the rocks can accelerate to a velocity of 5m/s under gravity. The velocity of the rocks can be related to the length of the pipe by the kinematic equation given below:

$$v^2 = 2gs + v_0$$

where v = final velocity

v_0 = initial velocity

g = acceleration due to gravity

s = distance of acceleration which gives the length of the pipe.

For $v_0 = 0$ and $g = 9.8 m/s^2$, the length of the pipe was found to be 1.27m.

4.5.2. Electronic circuitry.

Most of the circuitry was developed by A. de Waal (51,52). A more detailed discussion can be found in these references. In this thesis, only a brief overview of the circuitry and its application will be given. A block diagram of the circuitry is shown in figure 4.12 below.

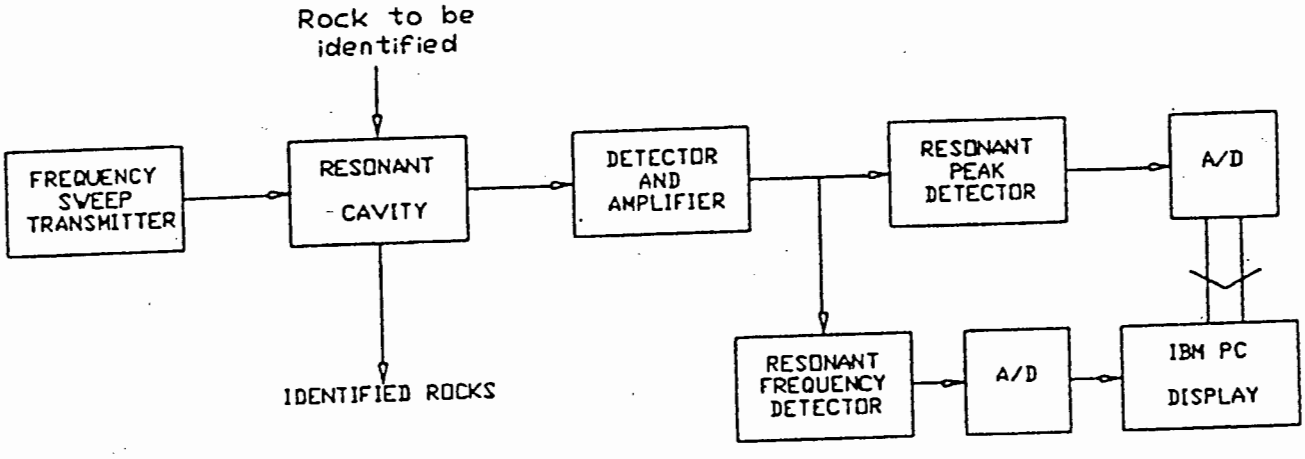

Fig 4.12 Block diagram of electronic circuitry.

The VCO frequency is swept up and down from about 475MHz to 495MHz with a triangular voltage wave form. This range covers the resonant frequencies for the three cases of unloaded cavity (f_{0u}), cavity loaded with gabbro (f_{0g}) and for the cavity loaded with kimberlite (f_{0k}). Only the case of the unloaded cavity will be discussed in explaining what happens as the VCO frequency is swept up and down. The cases for the loaded cavity are similar (53).

As the transmitter output is swept up in frequency, it approaches f_{0u} at which point the unloaded cavity resonates. A sharp peak in the transmission coefficient is observed. The peak detector gives a voltage v_{0u} proportional to the peak in transmission coefficient.

As the frequency sweeps past f_{0u}, v_{0u} drops sharply. The maximum output frequency is reached and a downward sweep begins. The same behaviour is observed when this frequency goes past f_{0u} again. Clearer understanding of this is facilitated by the waveforms shown in figure 4.13 below. The responses for the cavity loaded with a rock sample are also shown.

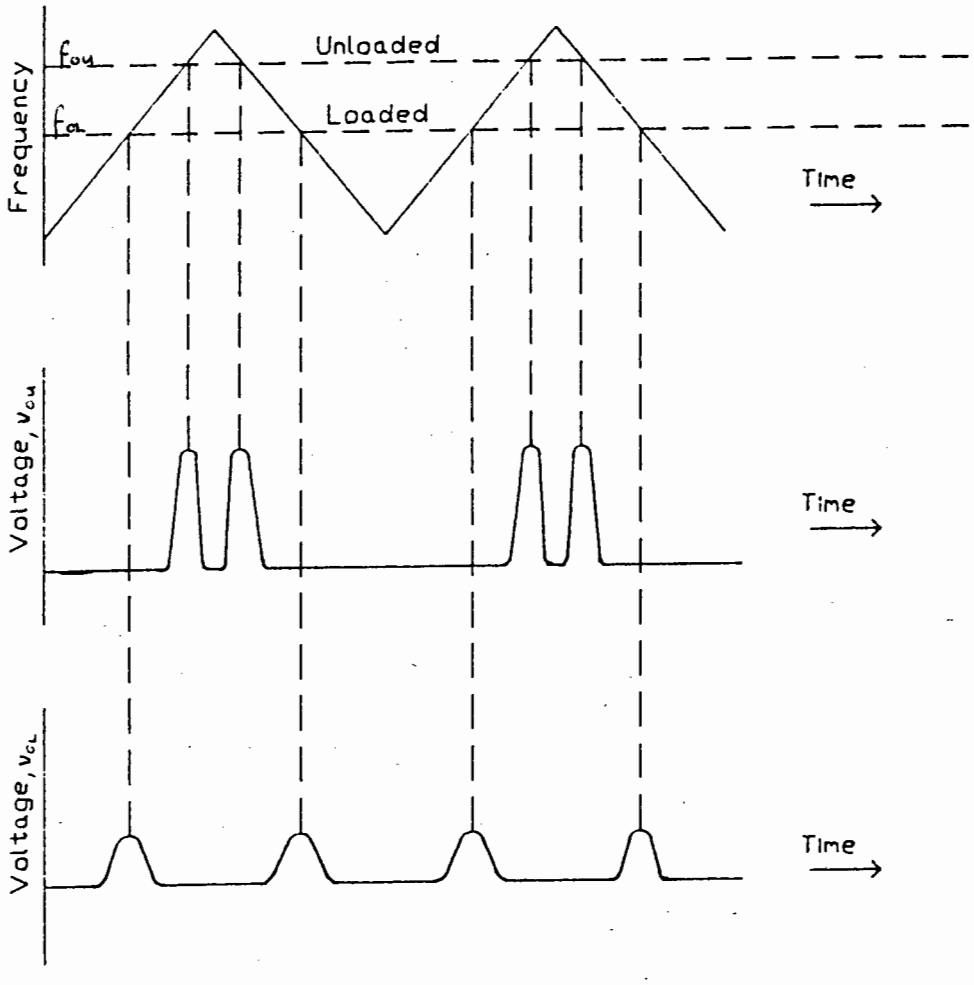

Fig 4.13 Waveforms observed at the transmitter and the peak detector outputs.

As can be seen from the figure above, the unloaded cavity has a higher peak v_0 which is proportional to the detected signal amplitude. It also has a lower period between peaks which is proportional to the change in resonance frequency. This means that the

signal amplitude and resonant frequency are less for the unloaded cavity than for the cavity loaded with either gabbro or kimberlite.
The detected peak voltages go into the analog to digital converter and into the IBM personal computer as discussed in the next subsection.

4.5.3. Data capture

An IBM personal computer (PC) was used to capture the data. This PC was fitted with a PC-26 analog to digital (A/D) converter card. The converter card is used to interface the analog outputs of the rock differentiation equipment to the digital inputs of the computer. A computer program used to process the input data was used (54). This program is shown in Appendix III.

4.5.4. Equipment operation

A diagram showing the equipment configuration is given in figure 4.14 below.

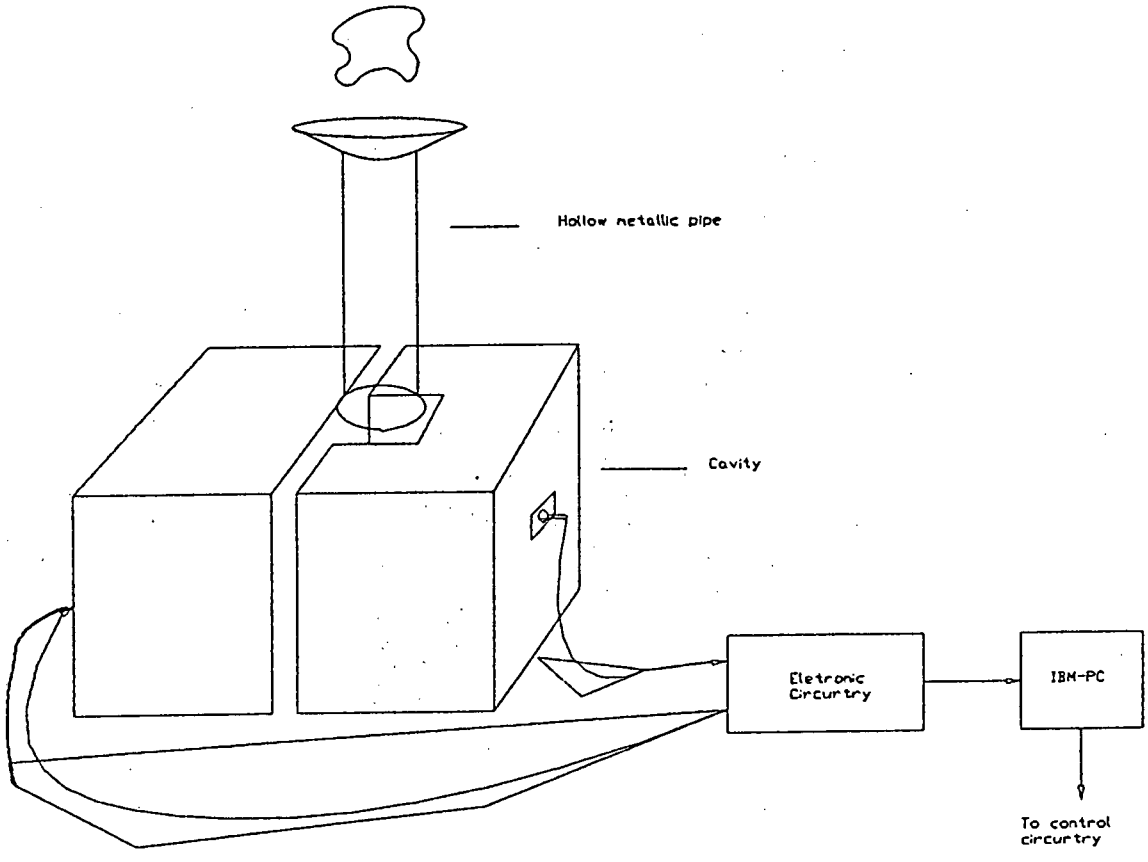

Fig 4.14 Set up for dynamic measurements.

A brief description of how the whole system operates is given below.

A rock sample is dropped through the cylindrical pipe. Its velocity as it enters the cavity is approximately 5m/s. As soon as the rock enters the cavity, the computer starts sampling. The information as to when to start sampling is transmitted to the computer by an optocoupler which detects the breaking of a light beam by a rock. The optocoupler arrangement is given by figure 4.15 below.

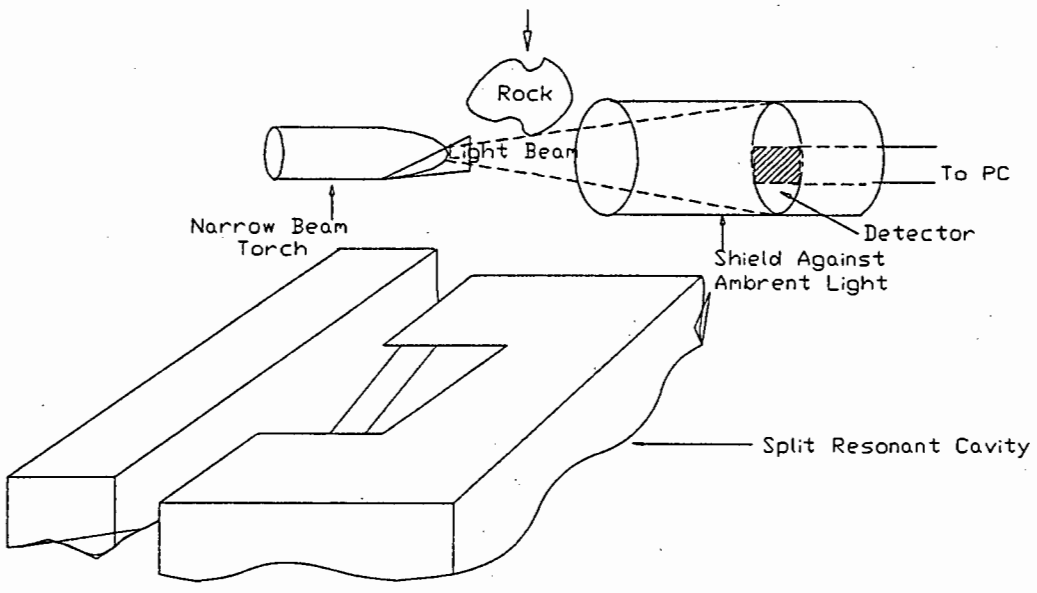

Fig 4.15 Optocoupler arrangement.

The rock then enters the cavity. It interacts with the microwave signal that is transmitted from the VCO. The resonant frequency and the Q-factor are reduced. The signal received on the other end of the cavity is detected by a microwave detector diode. This signal is then amplified and fed via the ADC into the PC. Unlike in the static case where the actual Q was measured, only the relative change in the resonant peak caused by each sample could be measured. The resonant peak amplitude is proportional to the cavity Q and could thus be used as effectively (55).

Based on the size of the reduction in the resonant peak, a threshold level has been established by measuring many ore samples above or below the threshold value, the PC would then either activate the air jets to blast the sample into the gabbro bin or leave it to fall freely into the kimberlite bin.

Results from the actual tests performed are given and discussed in the next two chapters. One chapter will deal with the results from the static tests while the other will be dealing with results from the dynamic tests.

5. ANALYSIS AND RESULTS OF STATIC TESTS

In this chapter, some of the results from the static tests will be presented and discussed. Even though the structure of prime importance is the split resonance cavity shown in figure 4.9, other cavities were also tested for comparison. Many measurements were taken on different cavity configurations with different loadings. Many of these configurations showed a performance not very different from the original closed cavity and the split cavity. Thus only results from three different cavities will be discussed. These are the closed cavity as shown in figure 5.1 A and the split cavities as shown in figures B and C below.

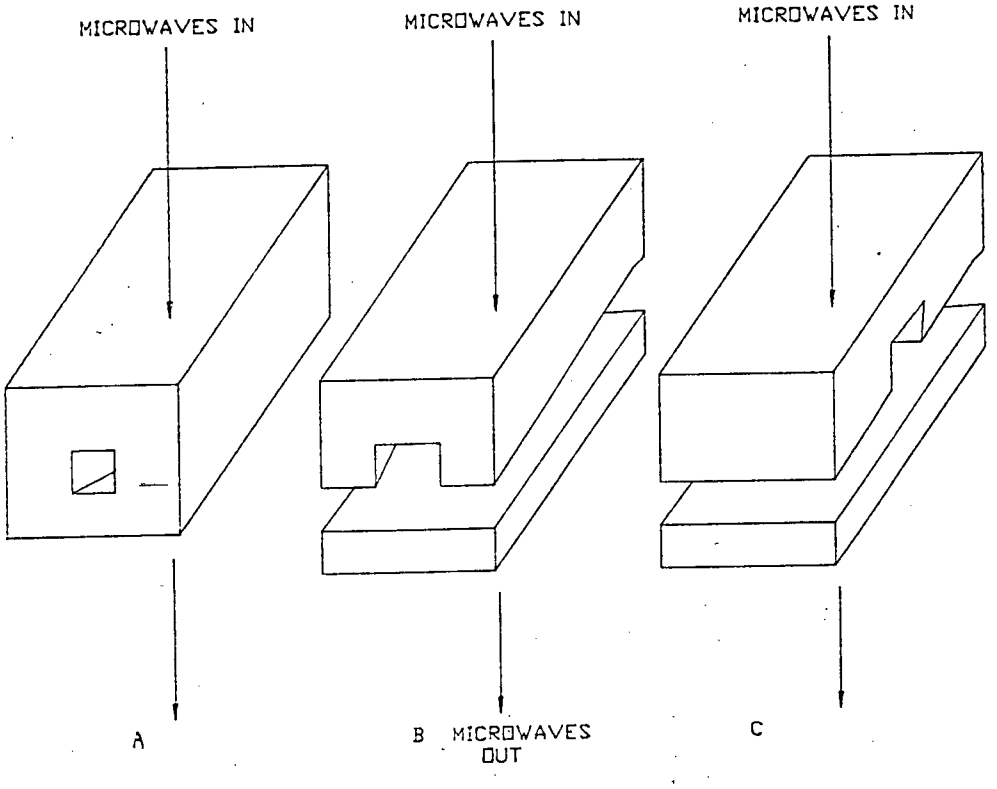

Fig 5.1 Resonant cavities for which results are given.

Cavity C was thought to be worth investigating because of the possible throughput increase that might be obtained (56). The distance between samples when using cavity C does not have to be as long as when either A or B are used. This means more rocks can be sorted per hour.

In the following sections measurements of unloaded cavities and cavities loaded with both the conveyor belt and rock samples will be discussed. Some conclusions on these tests will then be presented.

5.1. Measurements for cavity without conveyor belt.

Initial tests of the three cavities performance were made without the presence of the conveyor belt. This was done so that comparisons can be made for the cases where the conveyor belt is present. The two parts in cavities B and C are kept apart by thin strips of polystyrene of thickness 1cm. As mentioned before, the polystyrene hardly has any effect on microwave signals. Measurements for the empty cavities are given first, followed by measurements for cavities loaded with gabbro and kimberlite in turn.

5.1.1. Unloaded cavities.

The resonant frequency for frequencies at half-power points, f_1 and f_2, Q-factor and transmission coefficient S_{21}, for the three cavities are given in Table 5.1 below.

Cavity	f_0 [MHz]	f_1 [MHz]	f_2 [MHz]	Q	S_{21} [dB]
A	490.1	489.2	490.8	306	33
B	514.5	511.9	516.6	110	25
C	499.8	497.8	501.5	135	22

Table 5.1 Results obtained for the unloaded cavities.

As expected, the resonant frequency increases for the split cavities and the Q decreases. These effects are less for cavity C. This is because the rectangular slots for passing rocks through are cut on the faces where radiation is minimal (See Appendix II). Thus the radiation out of cavity C is intermediate between that in cavities A and B. This is evidenced by the respective values for Q.

5.1.2. Cavities loaded with rocks

The different cavities were then loaded with twelve samples of gabbro and twelve of kimberlite in turn. The results obtained are given in Table 5.2 and figs 5.2 - 5.4 below.

Cav	Kimberlite				Gabbro			
	f_0 [MHz]	f_1 [MHz]	f_2 [MHz]	Q	f_0 [MHz]	f_1 [MHz]	f_2 [MHz]	Q
A	482.6	481.2	484.1	168	488.7	487.8	489.5	288
	482.0	481.4	484.3	166	487.0	486.0	487.7	286
	484.1	483.0	485.8	173	488.8	488.0	489.7	292
	483.0	482.2	485.1	167	488.0	487.1	488.7	288
	482.4	481.0	483.9	165	488.9	487.7	489.4	291
	483.1	481.5	484.1	184	488.6	486.9	489.6	290
	483.7	482.3	485.1	171	486.9	485.3	487.1	278
	481.9	480.3	483.0	176	487.8	486.9	488.6	289
	482.2	481.2	484.0	172	488.1	487.1	488.8	285
	481.8	480.7	483.6	167	487.6	487.0	488.7	279
	480.5	479.3	482.1	170	488.0	486.2	487.9	284
	481.3	480.2	483.0	169	488.2	487.6	489.3	287
B	509.7	506.6	512.5	86	509.8	507.2	512.2	102
	509.5	506.6	512.5	86	508.9	506.6	511.5	104
	506.7	503.4	510.2	75	510.4	508.1	512.9	106
	507.5	504.4	511.1	76	511.0	508.7	513.6	104
	509.5	506.6	512.5	86	511.0	508.8	513.8	102
	507.3	503.8	510.8	73	509.1	506.9	512.0	100
	506.5	503.5	510.1	77	511.9	509.3	514.3	102
	506.5	504.0	510.1	83	511.4	508.8	513.9	100
	506.5	503.7	509.7	84	507.3	504.7	509.8	100
	504.2	500.6	507.8	70	511.3	509.0	514.0	102
	503.7	500.6	507.4	74	508.9	506.6	511.7	100
	504.0	501.3	507.4	83	511.2	508.9	513.8	104
C	493.0	490.5	495.5	99	496.4	494.1	498.6	110
	489.5	486.3	492.9	74	496.9	494.8	498.8	124
	494.1	491.7	496.7	99	495.9	493.8	497.8	124
	494.9	492.5	497.4	101	496.6	494.6	498.7	121
	493.7	491.2	496.4	95	496.6	494.6	498.6	124
	494.4	492.1	496.8	105	493.7	491.6	495.8	118
	491.4	488.9	494.1	95	494.6	492.5	496.8	115
	491.8	489.5	494.0	109	495.9	493.7	497.9	118
	492.0	488.9	495.4	76	496.3	494.1	498.3	118
	486.4	482.3	490.5	59	495.1	493.0	497.2	118
	488.8	485.6	492.5	71	494.5	492.5	496.7	118
	488.1	485.3	491.4	80	492.9	490.8	495.2	112

Table 5.2 Results obtained for cavities loaded with rocks.

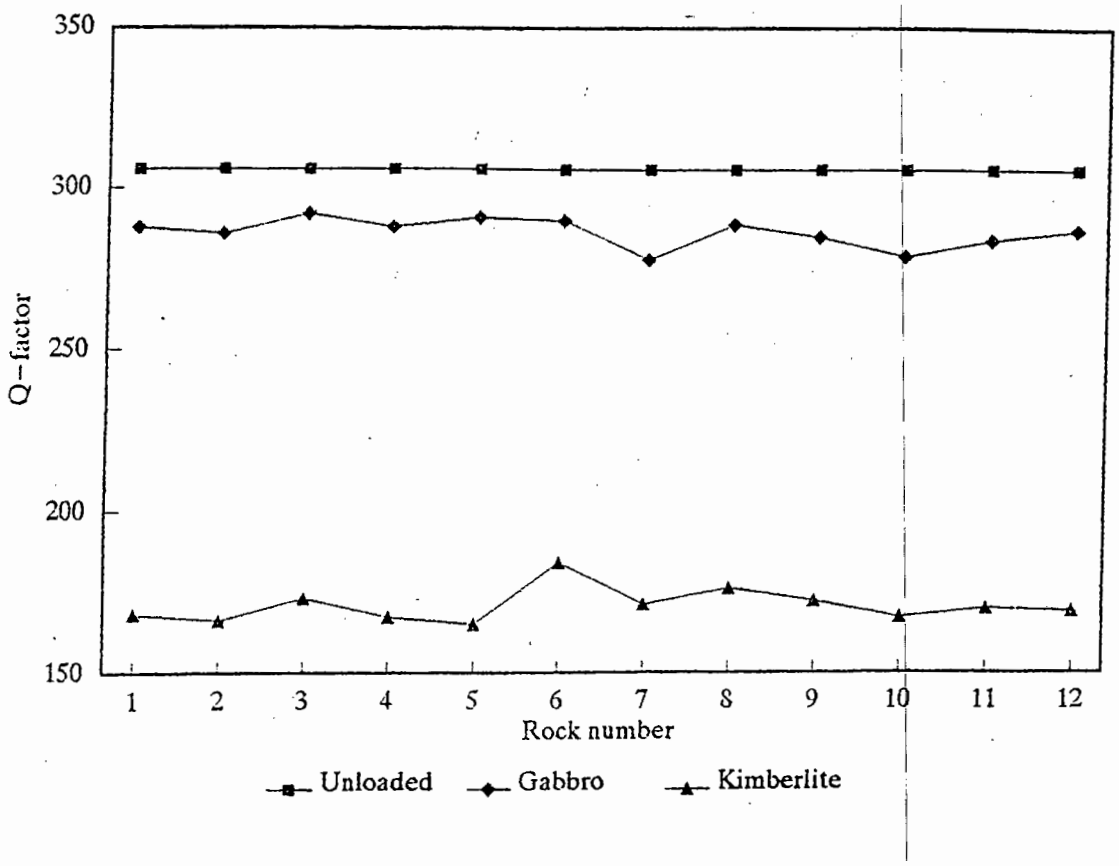

Fig 5.2 Q-factors for cavity A with different loads.

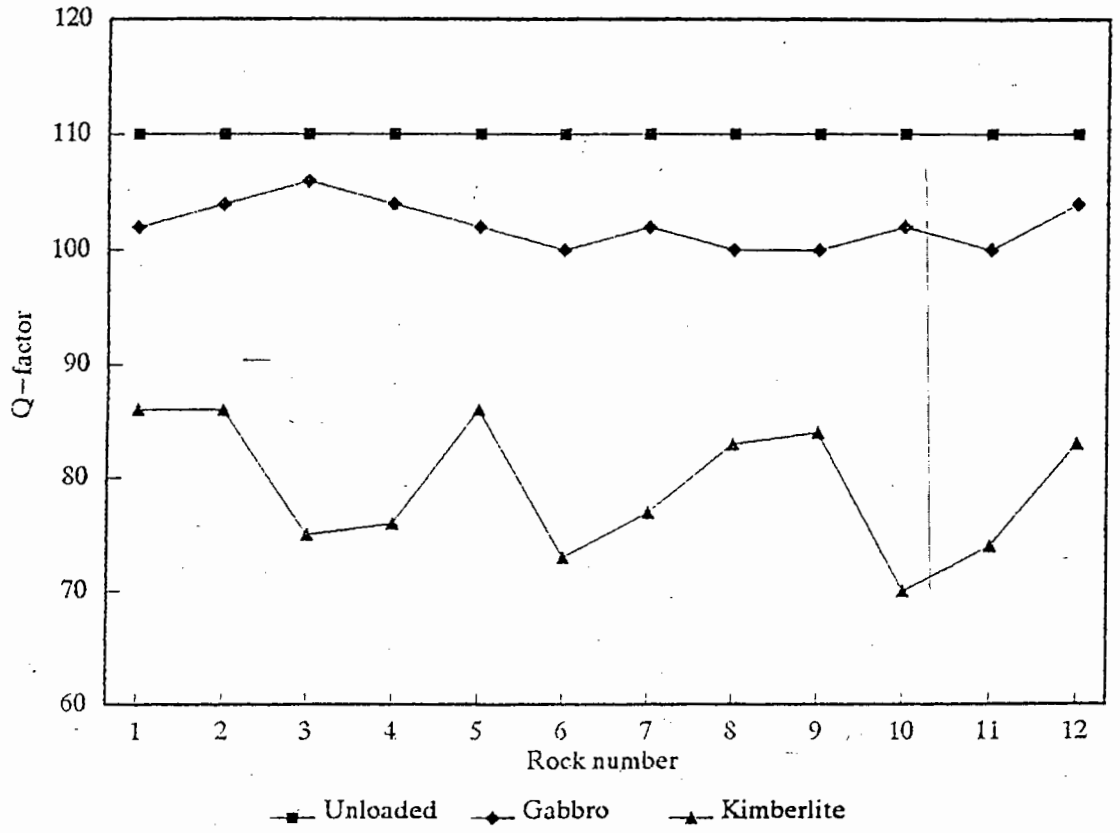

Fig 5.3 Q-factors for cavity B with different loads.

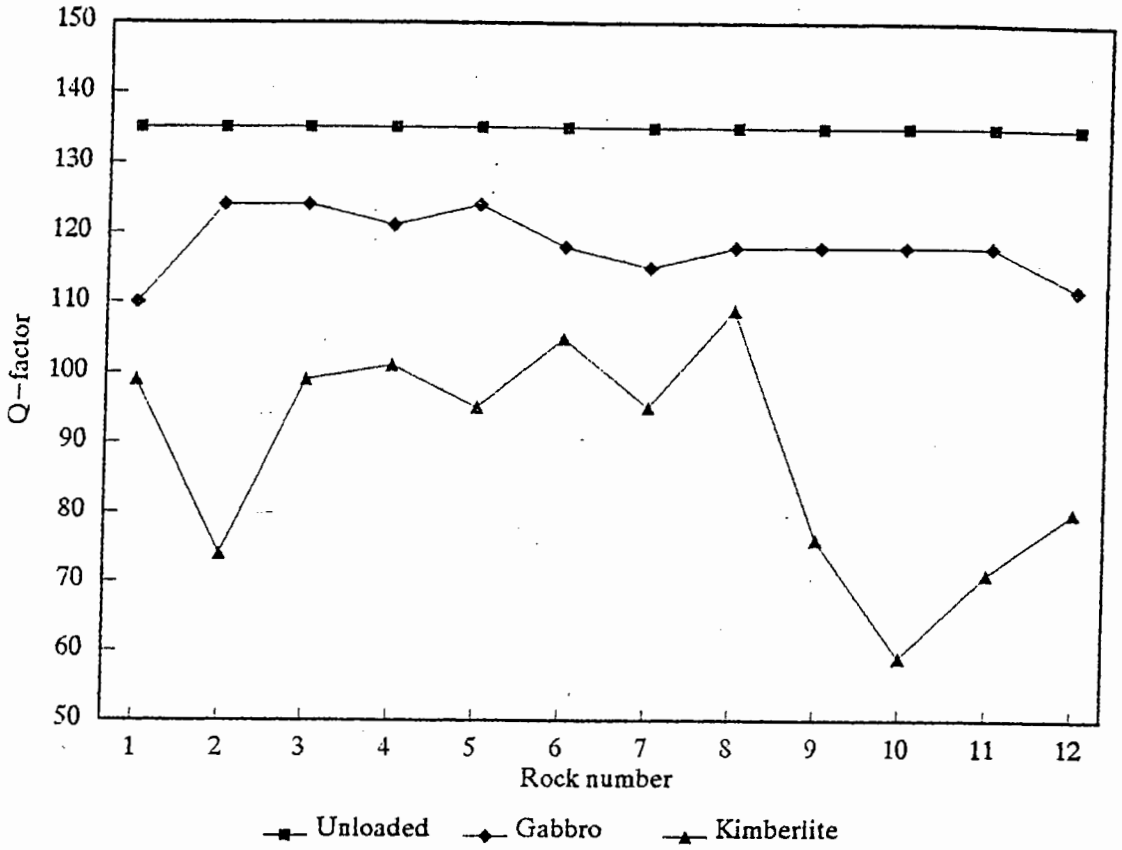

Fig 5.4 Q-factors for cavity C with different loads.

As can be seen from table 5.2 and figs 5.2 - 5.4 above, for each of the cavities, the Q found for the unloaded cavity is greater than the Q's found for gabbro. These, in turn, are greater than the Q's found for kimberlite. This shows that 100% separation of gabbro from kimberlite is achieved; even with the split cavities.

The results obtained are exactly as predicted in earlier chapters. The next step was to load the cavities with a strip of conveyor belt material. The results found for this case are discussed in the following section.

5.2. Measurements for cavities with conveyor belt

Strips of conveyor belt material of thickness 1cm were placed between the two resonant cavity parts. This was only done for cavities B and C. Cavity A was omitted because it can never be operated with a conveyor belt running through it.
The two cavities with the strip of conveyor belt are shown in figure 5.5 below.

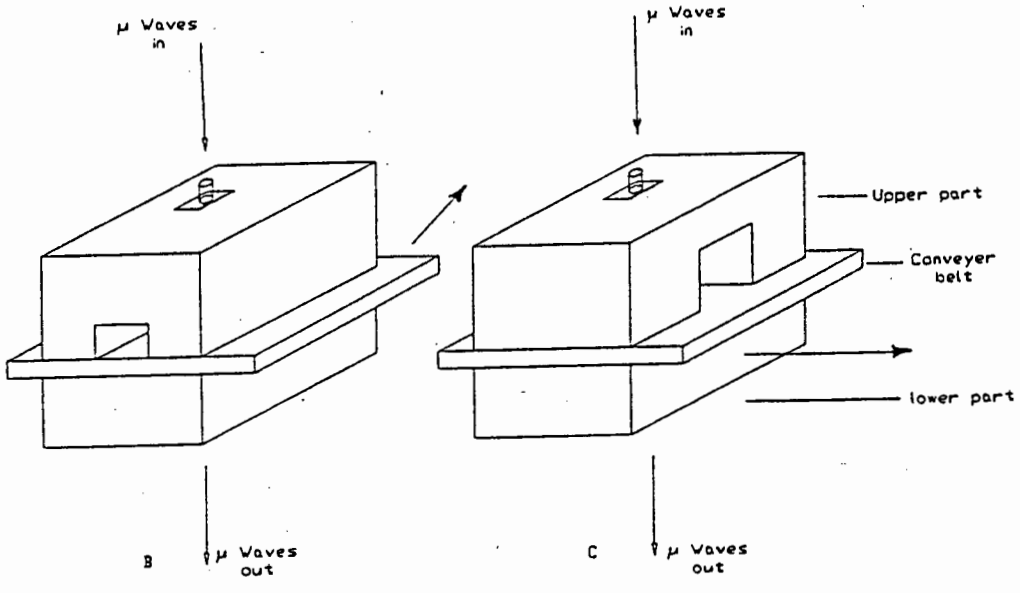

Fig 5.5 Cavities with strip of conveyor belt.

The directions in which the conveyor belt would be moving and the direction of propagation of the microwave signal in a real industrial plant are shown by the arrows. The results obtained for this arrangement are discussed in the subsections below.

5.2.1. Unloaded cavities

Measurements were taken first with only the conveyor belt loading the cavities ie. without any rock samples. The results obtained are given in Table 5.3 below.

Cavity	f_0 [MHz]	f_1 [MHz]	f_2 [MHz]	Q	S_{21}
B	437.8	424.3	447.4	19.0	15
C	433.3	423.8	444.0	21.5	12

Table 5.3 Results obtained for cavities loaded with conveyor belt.

Table 5.3 shows a large reduction in resonant frequency and Q as predicted. When compared to the case where the conveyor belt was not there, the Q was found to be 5.8 times lower for Cavity B and 6.3 times lower for C.

Results of tests performed to see if these cavities can still discriminate between the two rock types are given and discussed in the next subsection.

5.2.2. Cavities loaded with rocks

Samples of rocks were placed on top of the conveyor belt inside the cavity. As before, the relevant measurements were taken from the HP8412 magnitude and phase display module. These results are given in Table 5.4 and figs 5.6 and 5.7 below.

Cav	Kimberlite				Gabbro			
	f_0 [MHz]	f_1 [MHz]	f_2 [MHz]	Q	f_0 [MHz]	f_1 [MHz]	f_2 [MHz]	Q
B	431.0	418.1	442.9	17.2	434.2	423.0	443.9	20.6
	430.3	417.1	442.7	16.8	434.1	421.2	446.0	17.4
	428.2	415.0	441.0	16.5	433.4	420.9	445.1	18.0
	427.3	415.8	439.0	18.4	433.9	421.0	445.1	18.1
	428.1	415.8	440.5	17.3	432.9	421.1	443.9	18.8
	430.4	419.5	442.1	19.0	432.3	420.8	443.0	19.6
	430.0	418.1	442.1	17.9	433.1	421.2	443.8	19.2
	429.0	417.1	441.9	17.3	430.6	418.5	441.5	18.7
	429.8	417.3	442.2	17.3	431.6	419.8	441.4	20.0
	432.0	420.2	443.8	18.3	433.3	422.6	443.6	20.6
	431.8	419.2	444.0	17.4	432.6	421.1	443.6	19.2
	431.8	419.3	444.5	17.1	432.9	420.6	443.2	19.2
C	426.8	417.6	437.2	21.8	430.0	419.7	440.3	20.9
	426.5	416.2	437.4	20.1	431.3	421.3	440.8	22.1
	423.9	412.4	436.0	18.0	429.3	420.2	439.4	22.4
	426.9	415.9	438.1	19.2	428.8	419.1	438.6	22.0
	429.0	417.5	440.3	18.8	431.1	420.9	441.2	21.2
	427.1	416.5	437.5	20.3	429.9	420.7	439.7	22.6
	427.3	416.6	438.2	19.8	430.4	421.3	440.8	22.1
	424.3	413.0	435.1	19.2	429.9	420.3	440.6	21.2
	429.0	418.6	440.1	20.0	428.4	418.2	439.9	19.7
	428.9	417.9	439.0	20.3	430.8	421.0	440.6	22.0
	427.8	417.3	438.4	20.3	429.3	419.2	439.4	21.3
	424.6	413.4	437.0	18.0	430.6	421.0	440.8	21.7

Table 5.4 Results obtained for cavities loaded with both conveyor belt and rocks.

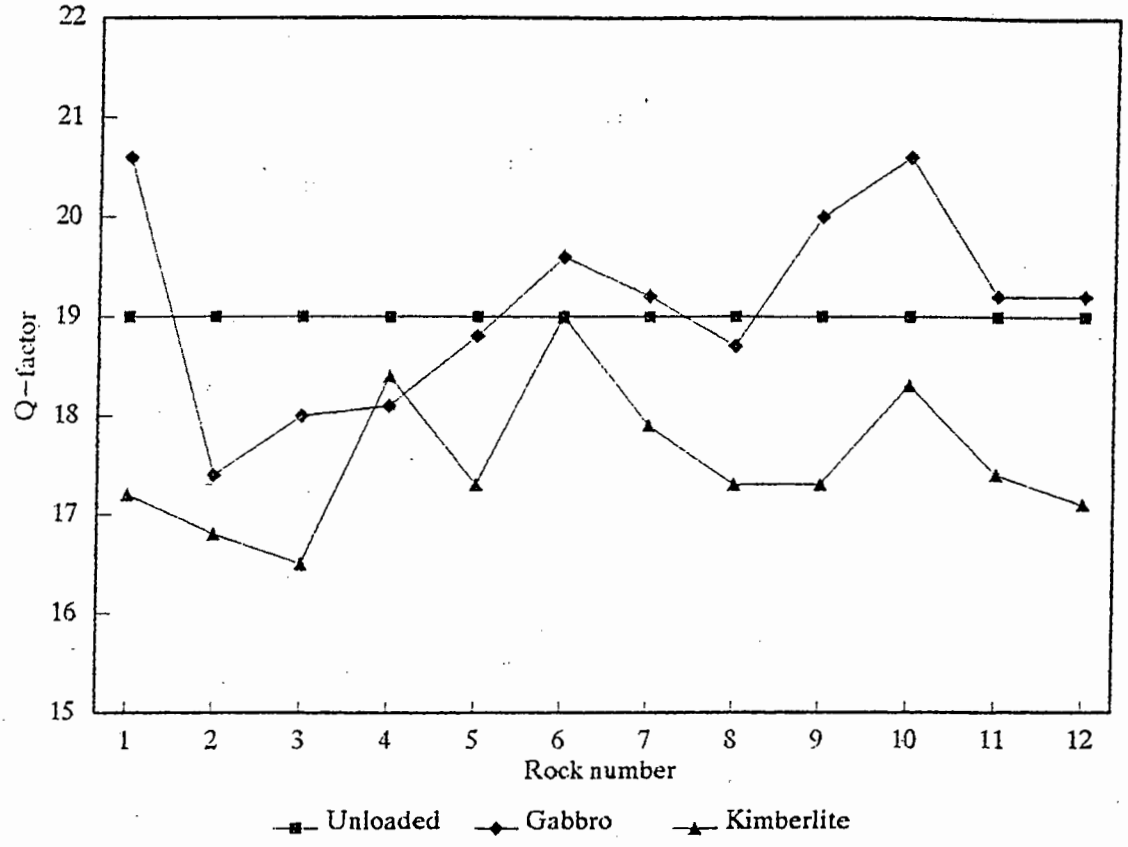

Fig 5.6 Q-factors for cavity B with different loads.

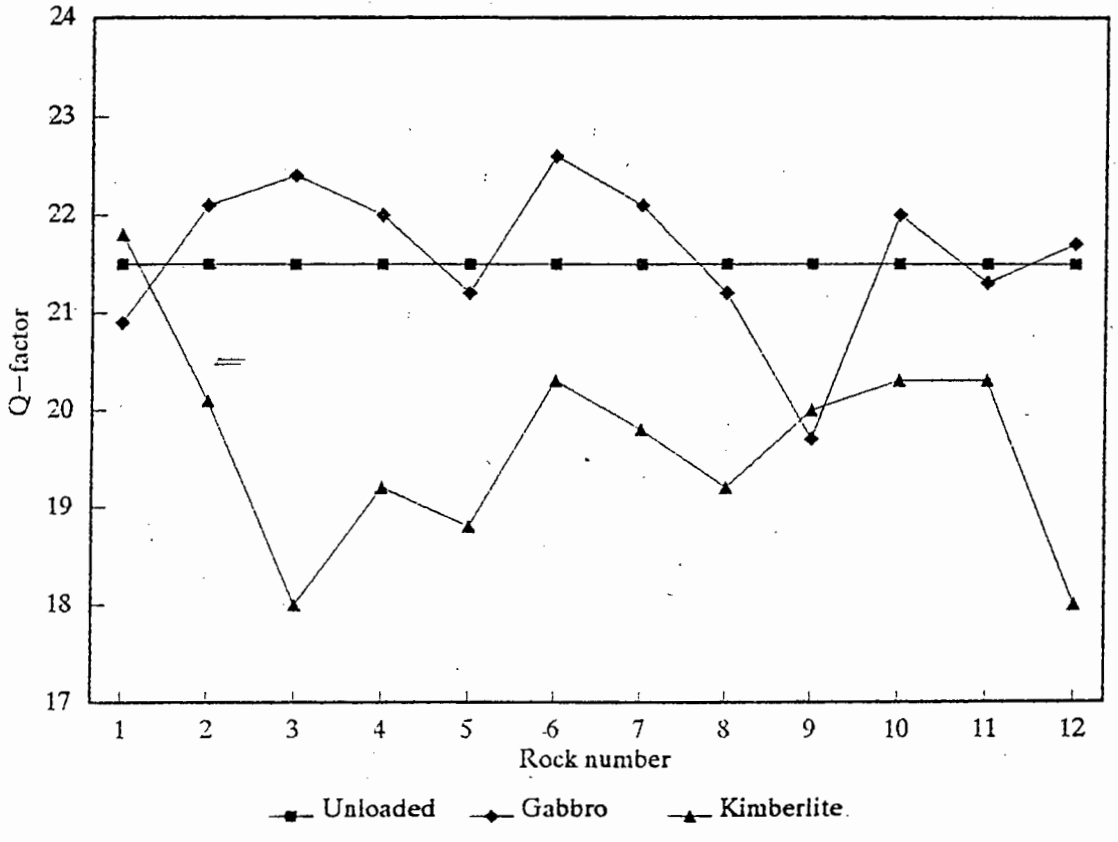

Fig 5.7 Q-factors for cavity C with different loads.

From table 5.4 and figs 5.6 and 5.7 above it can be seen that the Q's are so low that any further loading of the cavity does not lead to much change. For cavity B, if the separation threshold is set to Q = 19.0 to ensure correct identification of all the kimberlites, 5 out of 12 gabbros will be wrongly identified. This is an accuracy of only 58.3%. Cavity C gives mis-identification of 6 gabbros out of 12 when the threshold is set to Q = 21.8. This gives exactly 50% accuracy.

5.3. Conclusions on static tests.

From the preceeding sections the following conclusions may be drawn:

1. All cavities show perfect discrimination when there is no conveyor belt.
2. The best and worst performance is observed for Cavity A and B respectively. Therefore, it can reasonably be assumed that if Cavity C were not split into two, it would have a performance that is even better than A's. Not only would it be more accurate, it would also be faster; as discussed at the beginning of Chapter 5.
3. The conveyor belt material drastically reduces the Q. This means this material is very lossy to microwaves. In its presence, effects of other materials that might change the Q are hardly noticeable.
4. The conveyor belts used were supplied by the De Beers Diamond Research Laboratory and are the actual belts which are used in diamond mines. The conveyor belt materials are chosen for good wear properties. If the system using split cavity is to be viable a new low loss material for manufacturing conveyor belts would be required.

In the next chapter, results from dynamic tests will be presented and discussed.

6. ANALYSIS AND RESULTS FOR DYNAMIC TESTS

The three resonant cavities described in chapter 5 were also used in this chapter. Each of the cavities was connected to the test equipment as shown in figure 4.12.

The electronic circuitry and the PC were used to collect the measurement data. Two traces obtained from the data input into the PC were displayed on the screen. One trace was from the resonant peak detector circuitry data and the other was from the resonant frequency detector data.

When the cavity was loaded with rocks in the absence of a conveyor belt, the traces were observed to dip and have trough like shapes. This corresponds to the path of the rock through the resonant cavity with the maximum attenuation and frequency occurring in the centre of the cavity where the **E**-field is a maximum. Potentiometers in the electronic circuitry were set such that reasonable traces were observed; as shown in figure 6.1 below.

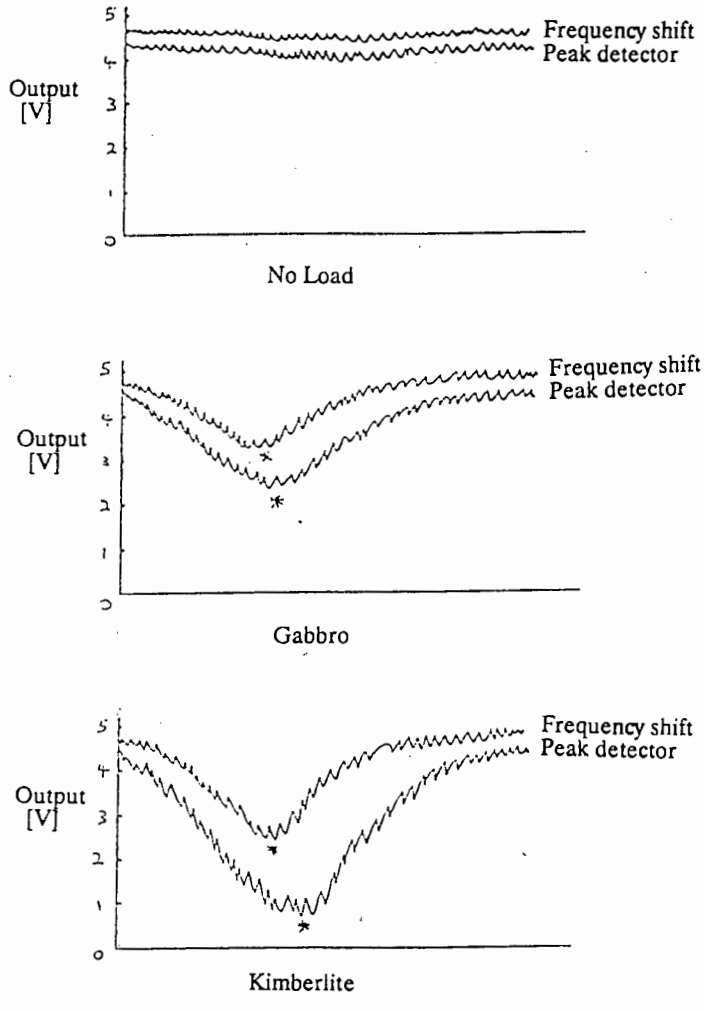

Fig 6.1 Traces observed on screen for different loads.

The diagrams above show:

- level traces for both frequency shift and peak detector output when there is no rock inside the cavity.
- dips in both traces with the frequency shift trace dipping lower when a sample of gabbro is dropped through the cavity.
- even larger dips when a kimberlite sample is dropped through.

- the difference in the frequency shift traces is not very pronounced when gabbro and kimberlite pass through the cavity but the differences in the attenuation (Q-factor) is substantial.

From these observations it is concluded that the peak detection method is the more reliable method for sorting the two rock types and results in a 100% separation.

The minimum voltage values, marked by * in figure 6.1, are stored in the PC. These values are the results that are presented and discussed in the rest of this chapter. The results are presented first for the cavity without the conveyor belt. Observations when the belt was introduced into the cavity are also presented. Some conclusions on dynamic tests are then drawn.

6.1. Measurements for cavity without conveyor belt

The measurements obtained for the three unloaded cavities i.e. in the absence of the conveyor belt when discrete rock samples are passed through at 5 m/s are presented in this sub-section. These are given in Table 6.1 below and are also shown graphically in figs 6.2 - 6.4. As mentioned earlier, potentiometers in the electronic circuitry were arbitrarily set in such a way as to ensure that the range of values was between 0V and +5.5V for different samples. Thus comparisons cannot be made between cavities; only between rock types for a given cavity. It must be noted that in this table, higher voltage values represent smaller changes in both the amplitude and the resonant frequency. Therefore it is expected that the values obtained for kimberlite should be lower.

	Kimberlite		Gabbro	
Cavity	Amplitude minimum [V]	f_0 minimum [V]	Amplitude minimum [V]	f_0 minimum [V]
A	2.37	3.00	4.54	4.02
	2.90	3.29	4.51	4.05
	1.43	2.56	4.67	4.46
	2.57	3.17	4.85	4.18
	3.02	3.36	4.02	2.53
	2.23	3.11	4.75	3.70
	2.59	3.14	4.97	4.34
	1.72	2.71	5.03	4.04
	2.22	2.88	5.13	4.65
	1.70	2.70	4.80	3.56
	1.90	2.96	4.96	4.35
	2.34	3.07	5.12	4.57
B	1.87	3.35	5.29	4.45
	2.53	3.50	5.28	4.73
	3.17	3.90	5.19	4.18
	3.13	3.55	5.36	4.84
	3.11	3.76	5.26	3.93
	3.41	2.71	5.11	3.88
	1.97	3.50	4.85	4.27
	2.37	3.17	5.30	4.57
	2.89	3.34	5.30	4.60
	2.28	3.11	5.22	4.19
	1.34	2.12	4.72	3.58
	3.38	4.14	5.15	4.07
C	1.46	2.75	2.66	3.39
	0.88	1.98	2.87	4.43
	1.10	2.86	2.46	3.10
	1.80	3.41	2.58	2.77
	1.06	2.46	2.68	3.61
	1.78	3.29	2.59	2.92
	1.09	1.85	2.61	3.47
	0.96	2.43	2.72	3.55
	1.22	2.81	2.19	2.83
	1.49	2.30	2.39	3.43
	1.73	2.59	3.21	4.44
	0.73	2.02	2.22	3.03

Table 6.1 Minima for cavities loaded with rocks.

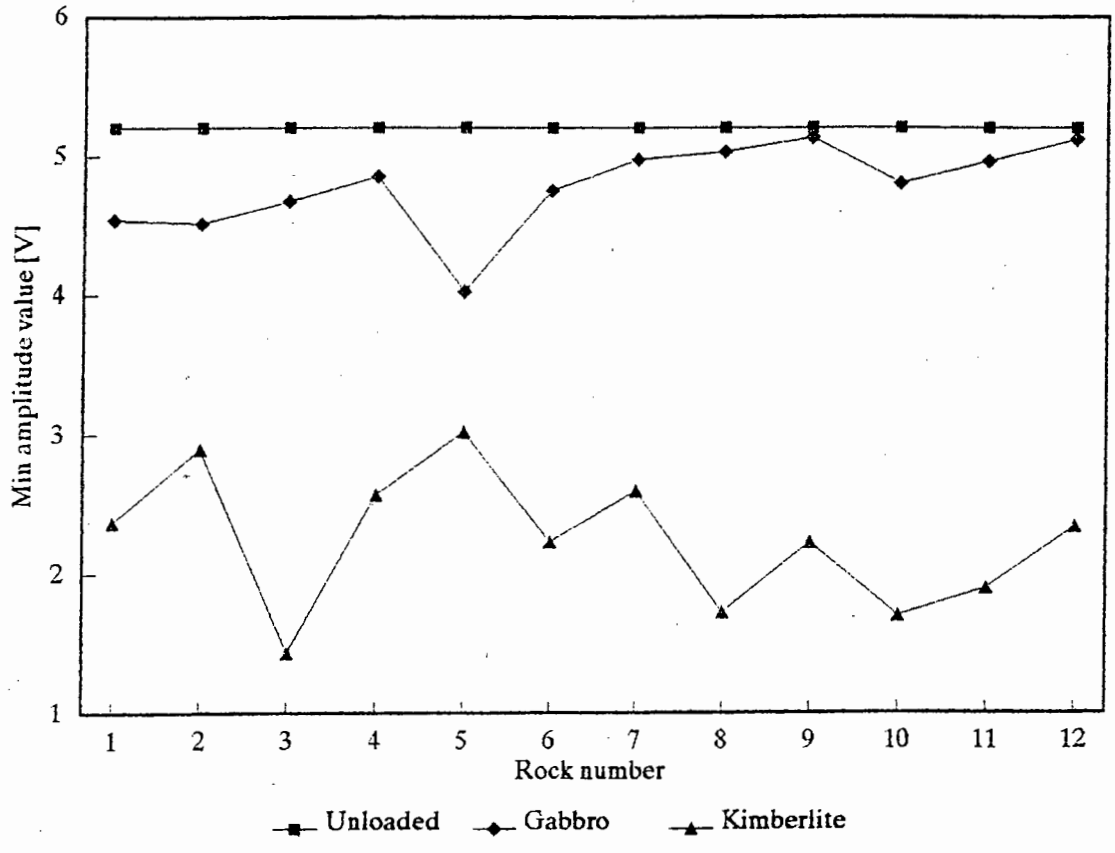

Fig 6.2 Minimum voltage values for cavity A with different loads.

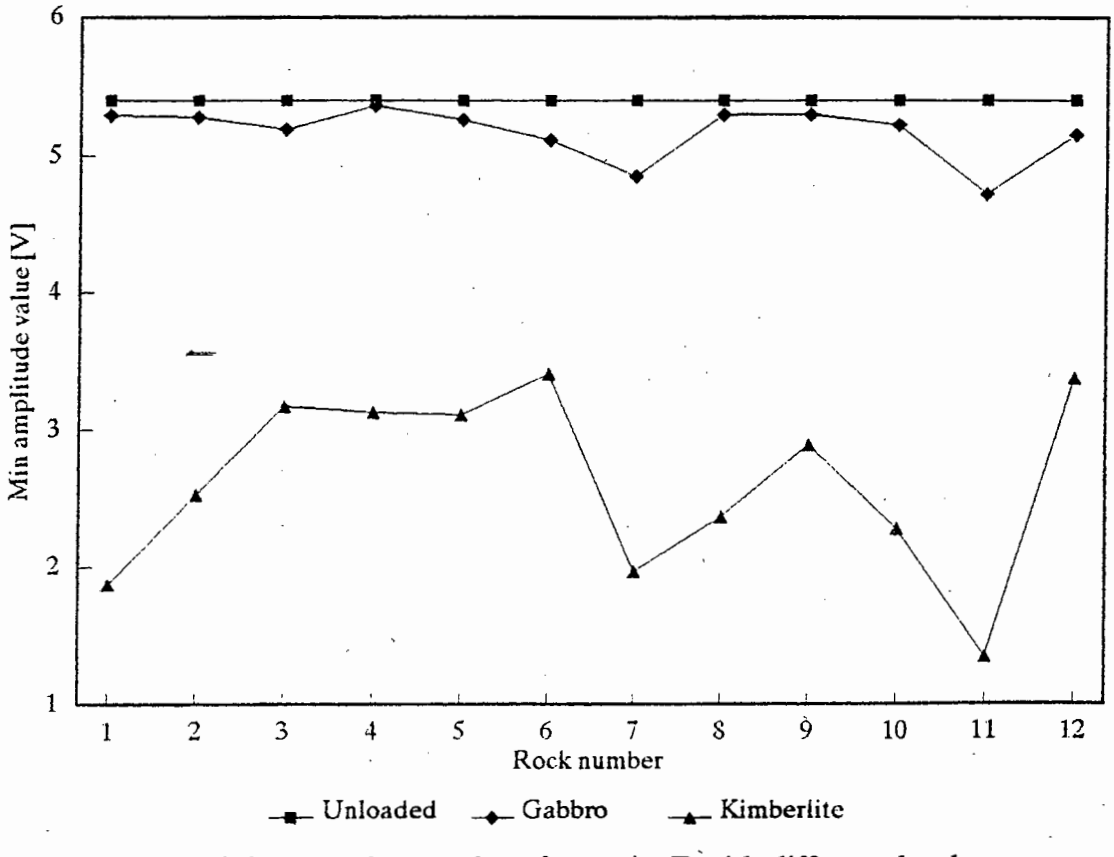

Fig 6.3 Minimum voltage values for cavity B with different loads.

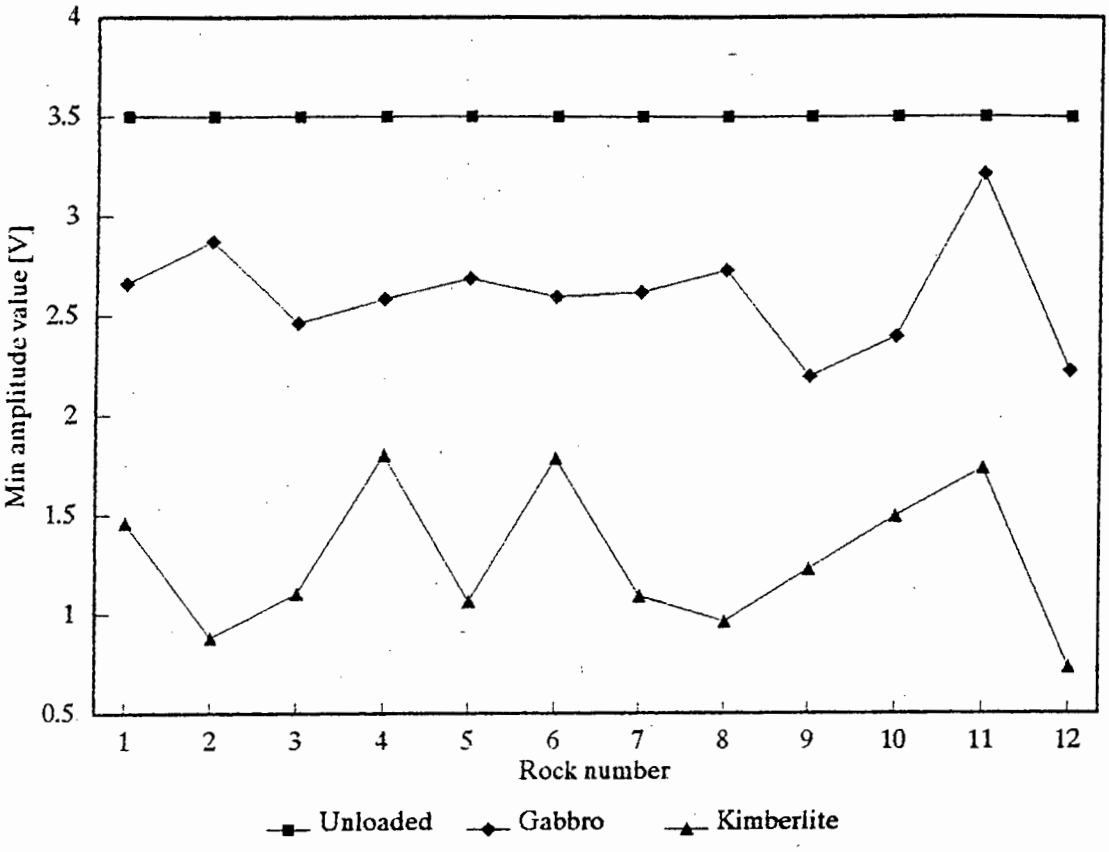

Fig 6.4 Minimum voltage values for cavity C with different loads.

6.2. Observations for cavity with conveyor belt

Strips of conveyor belt material were inserted into the cavities as in the static tests. The equipment used was exactly the same as in tests without the conveyor belt material. The following traces were observed on the PC screen:

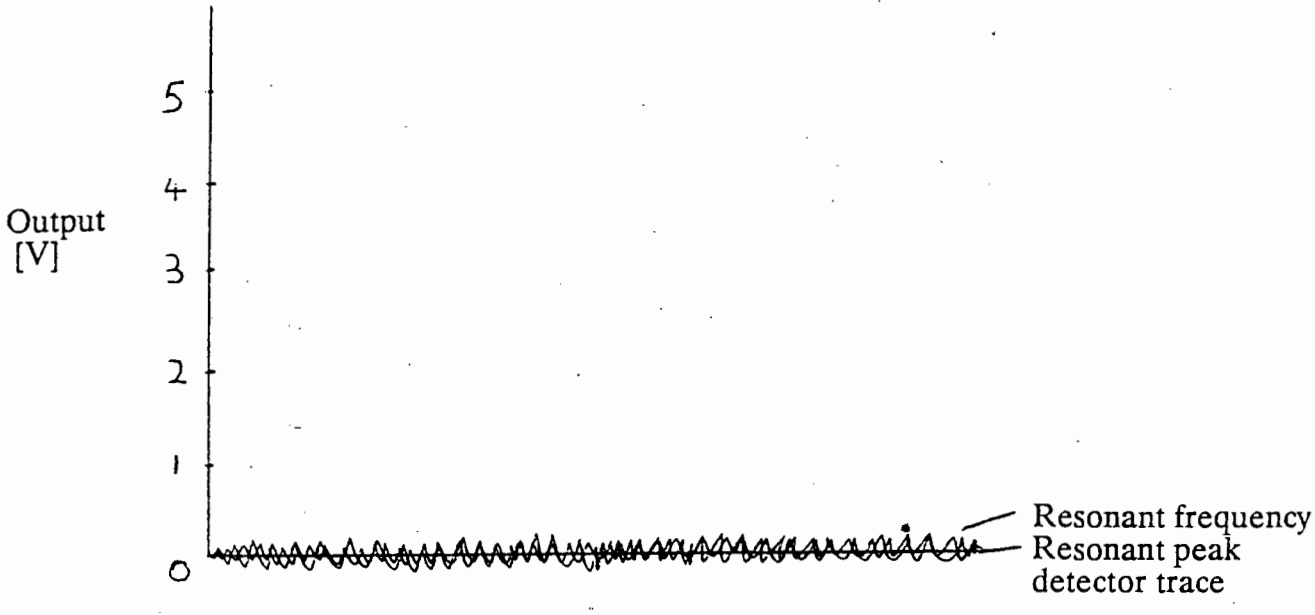

Fig 6.5 Traces observed for cavity with conveyor belt.

The traces were at 0V as shown in figure 6.5. Different potentiometer settings had no effect on these traces. An oscilloscope was used to check the signal at different points in the electronic circuitry. It was found that the signal received at the receiver end was quite small i.e. of the order of a few hundredths of a microvolt. This was of the same order of magnitude as the noise. A 60dB gain in the amplifier stage only led to large amplification of both signal and noise. This rendered the signal unusable.

6.3. Conclusions on dynamic tests

The following conclusions can be drawn from the observations made in dynamic tests.

1. The change in the amplitude of the resonance peak can be used successfully to identify and sort the different rock types.
2. All three cavities showed good performance in the absence of the conveyor belt.

3. **Insertion of the conveyor belt drastically reduces the Q factor of the cavity and** absorbs the microwave signal such that almost nothing is received on the receiver end. The reasons for this are discussed in section 4.3.3

7. CONCLUSIONS AND RECOMMENDATIONS

Microwave equipment to differentiate between samples of gabbro and kimberlite on a rock by rock basis was constructed and tested.

Different microwave structures that could be used in the separation were considered. Many of them were discarded because of one or more of the following reasons: inaccuracy in separating, physical impracticality, excessive radiation and limited sensitivity to changes in the dielectric constant.

A structure which was a compromise between an open structure similar to horn antennas and a closed resonant cavity was chosen. This was a rectangular resonant cavity split into two halves with small non-radiating slots to pass the samples through. Loop coupling was chosen to couple energy into and out of the cavity. A resonant frequency of about 500MHz was chosen.

Both static and dynamic tests were performed on different rock samples with and without conveyor belt material. For the dynamic tests, a conveyor belt system travelling at 5m/s was simulated. Without the conveyor belt material, 100% separation of gabbro from kimberlite was achieved. With the conveyor belt this figure dropped to 58% in the static tests. In dynamic tests, no signal was received on the receiver end.

It is therefore recommended that different conveyor belt materials that have less attenuation to microwave signals be developed. These materials should however have relatively similar wear properties to those of the present conveyor belt. Also, equipment to measure the resonant frequency and the bandwidth on-line should be developed to give a more accurate measure of the Q-factor.

LIST OF REFERENCES

1. *South Africa 1988-1989*, Official yearbook of the Republic of South Africa, Ed. Bureau of Information, Cape Town: CTP Printers, 1989.

2. Cornelius S., Hurlbut J. R. and Cornelis K., *Manual of Mineralogy,* New York: John Wiley and Sons, 1977, p145.

3. Mercer S., *Rock Differentiation using Microwave irradiation,* MSc Thesis, Department of Electrical and Electronic Engineering, UCT, 1987, p2

4. Parkhomenko E.I., *Electrical Properties of rocks,* New York: Plenum Press, 1967.

5. Ramo S. et al, *Fields and waves in communication electronics,* 2nd ed, USA: John Wiley and Sons, 1967, p131.

6. Smyth C.P., *Dielectric Behaviour and Structure,* International Chemical Series, USA: McGraw-Hill, 1955, p52.

7. Rose R.M. et al, *Electronic properties,* vol IV, The structure and properties of materials, USA: John Wiley and Sons, 1966, p257.

8. Katz H.W., ed, *Solid State magnetic and dielectric devices,* USA:John Wiley and Sons, 1959, p69.

9. Rose R.M. et al, *Electronic properties,* vol IV, The structure and properties of materials, USA: John Wiley and Sons, 1966, p257.

10. Smyth C.P., *Dielectric Behaviour and Structure,* International Chemical Series, USA: McGraw-Hill, 1955, p15.

11. Parkhomenko E.I., *Electrical Properties of rocks,* New York: Plenum Press, 1967, p19.

12. Tarkhov A. G., *The relation of the dielectric constants of rocks to their mineral composition,* Izv. Akad. Nauk SSSR, Ser Geogr. i Geofiz., no 2, 1947.

13. Povarennykh A. S., *The dielectric constants of minerals*, Sci. Works Krivorog. Min. Inst., vol 8, 1960.

14. Roshkova E.V. and Proskurovskii L. V., Determination of the dielectric constants of minerals, Contemporary methods of mineralogic studies of rocks, ores and minerals, Gosgeoltekhizdat, 1957.

15. Pozar D.M., *Microwave Engineering,* USA: Addison-Wesley Publishing company, 1990, p343.

16. Pozar D.M., *Microwave Engineering,* USA: Addison-Wesley Publishing company, 1990, p265.

17. Montgomery C., *Techniques of Microwave Measurement,* M.I.T. Radiation laboratory series, USA: McGraw-Hill, 1947.

18. Kajfez D., *Influence of an airgap on the measurement of dielectric constants by a parallel-plate dielectric resonator,* IEE Proceedings Part H, v 133, n 4, (Aug 1986), p253-258.

19. Sanchez M.C., *Automatic technique for the characterization of a dielectric resonator coupled to a microstrip line,* IEE Proceedings Part H, v 133, n 2, (Apr 1986), p99-102, p159-161.

20. Zheng W., *Complex resonant frequencies of open composite dielectric resonators,* European Microwave conference : Microwave 87, Rome, Italy, Published by Microwave Exhibitions and Publications, Turnbridge Well, England, (1987), p945.

21. Roberts J., *Dielectric response of material media using the detuning of a resonant microwave cavity,* Microwave Power Electromagn, v 22, n 3, (1987), p185-186.

22. Magerl G., *Novel method for cavity parameter measurement,* IEEE Trans Instrum Meas, v IM-25, n 2, (Jun 1976), p145-151.

23. Parkhomenko E.I., *Electrical Properties of rocks,* New York: Plenum Press, 1967, p19.

24. Keller G.V., *Supplementary guide to the literature on Electrical properties of rocks and minerals,* p286

25. Horner F. et al, *Resonant methods of Dielectric Measurements at centimeter wavelengths,* IEE, 93, (Part 3,21), p53-68.

26. Lakshminarayana M.R. et al, *Simple microwave technique for independent measurement of sample size and dielectric constant,* IEEE Transactions, MTT-27, (1979), p661-665.

27. Kumar A. and Smith G., *Microwave properties of yarns and textiles using a resonant microwave cavity,* IEEE Transactions IM-26, (1977), p95-98.

28. Tanabe E. and Joines W. T., *A non-destructive method for measuring the complex permittivity of dielectric materials at microwave frequencies using an open transmission line resonator,* IEEE Transactions on Instrum. Meas., vol IM-25, (1976), p222-226.

29. Lyttle R.J., *Measurement of earth medium electrical characteristics: techniques and applications,* IEEE Transmissions on Geo Science Electron, vol 12, no 3, (1974), p81-101.

30. Webb W. E. and Church R. H., *Measurement of dielectric properties of minerals at microwave frequencies.* Report of investigations 9035, United States Bureau of mines, 1986.

31. Chope H. R., *Methods and apparatus for measuring multiple properties of material by applying electric fields at multiple frequencies,* US Patent 3.155.898, 1965.

32. Krazewski A., *Microwave aquametry-A bibliography for 1955-1979,* Journal of Microwave Power, v 15, n 4, (1980), p298-310.

33. Smyth C.P., *Dielectric Behaviour and Structure,* International Chemical Series, USA: McGraw-Hill, 1955, p202.

34. Booi M., *Ore sorting using microwave irradiation,* MSc Thesis, Department of Electrical and Electronic Engineering, UCT, 1989, piii

35. Booi M., *Ore sorting using microwave irradiation,* MSc Thesis, Department of Electrical and Electronic Engineering, UCT, 1989, p88-95.

36. De Waal A., *Rock differentiation using the properties of resonant waveguide cavities at 500MHz,* Unpublished 4th year Thesis, Department of Electrical and Electronic Engineering, UCT, 1987, p2.6.

37. Radebe K. G., *Investigation of transmission line resonant structures and development of associated measuring techniques for rock sorting,* Unpublished 4th year Thesis, Department of Electrical and Electronic Engineering, UCT, 1988, p6.

38. Mercer S., *On-line Microwave measurement of complex dielectric constant,* PhD Thesis, Department of Electrical and Electronic Engineering, UCT, 1990, p110

39. Liao S.Y., *Microwave Circuit Analysis and Amplifier Design,* New Jersey: Prentice-Hall, 1987, p197.

40. Ramo S. and Whinnery J. R., *Fields and waves in modern Radio,* USA: John Wiley and Sons, 1947, p292.

41. Pozar D.M., *Microwave Engineering,* USA: Addison-Wesley Publishing company, 1990, p183.

42. Harvey A.F., *Microwave Engineering,* Great Britain: John Wright and Sons Ltd, 1963, p407.

43. Liao S.Y., *Microwave Circuit Analysis and Amplifier Design,* New Jersey: Prentice-Hall, 1987, p198.

44. Mehdizadeh M. et al, *Loop-gap resonator: A lumped mode microwave resonant structure,* IEEE Transactions on microwave theory and techniques, vol 31, (1983), p1059.

45. Harvey A.F., *Microwave Engineering,* Great Britain: John Wright and Sons Ltd, 1963, p197.

46. Pozar D.M., *Microwave Engineering,* USA: Addison-Wesley Publishing company, 1990, p252.

47. Pozar D.M., *Microwave Engineering,* USA: Addison-Wesley Publishing company, 1990, p38.

48. Green W.J. and Verne S., *Natural and Synthetic Rubbers,* Ed. J.B. Birks, London: Heywood and Company, 1960, p84-85.

49. Broughton H. H., *The Electrical Handling of Materials,* Machinery and methods vol 4, London: Ernest Benn Limited, 1923, p42.

50. Smyth C.P., *Dielectric Behaviour and Structure,* International Chemical Series, USA: McGraw-Hill, 1955, p188.

51. De Waal A., *Rock differentiation using the properties of resonant waveguide cavities at 500MHz,* Unpublished 4th year Thesis, Department of Electrical and Electronic Engineering, UCT, 1987, p5.1.

52. Mercer S., *On-line Microwave measurement of complex dielectric constant,* PhD Thesis, Department of Electrical and Electronic Engineering, UCT, 1990, p110

53. De Waal A., *Rock differentiation using the properties of resonant waveguide cavities at 500MHz,* Unpublished 4th year Thesis, Department of Electrical and Electronic Engineering, UCT, 1987, p5.2.

54. Pascal computer program obtained from the Minerals Processing Division, De Beers Research Laboratory, Johannesburg.

55. De Waal A., *Rock differentiation using the properties of resonant waveguide cavities at 500MHz,* Unpublished 4th year Thesis, Department of Electrical and Electronic Engineering, UCT, 1987, p4.4.

56. Radebe K. G., *Investigation of transmission line resonant structures and development of associated measuring techniques for rock sorting,* Unpublished 4th year Thesis, Department of Electrical and Electronic Engineering, UCT, 1988, p38.

BIBLIOGRAPHY

Birks J.B., *Modern Dielectric Materials,* Ed. J.B. Birks, London: Heywood and Company, 1960.

Booi M., *Ore sorting using microwave irradiation,* MSc Thesis, Department of Electrical and Electronic Engineering, UCT, 1989.

Broughton H. H., *The Electrical Handling of Materials,* Machinery and methods vol 4, London: Ernest Benn Limited, 1923.

Chope H. R., *Methods and apparatus for measuring multiple properties of material by applying electric fields at multiple frequencies,* US Patent 3.155.898, 1965.

Cornelius S., Hurlbut J. R. and Cornelis K., *Manual of Mineralogy,* New York: John Wiley and Sons, 1977.

De Waal A., *Rock differentiation using the properties of resonant waveguide cavities at 500MHz,* Unpublished 4th year Thesis, Department of Electrical and Electronic Engineering, UCT, 1987.

Green W.J. and Verne S., *Natural and Synthetic Rubbers,* Ed. J.B. Birks, London: Heywood and Company, 1960.

Hanson D.F., *Microwave resonators,* Dielectric Resonators, Eds. D. Kajfez and P. Guillon, Norwood,MA: Artech House, 1986.

Harvey A.F., *Microwave Engineering,* Great Britain: John Wright and Sons Ltd, 1963.

Horner F. et al, *Resonant methods of Dielectric Measurements at centimeter wavelengths,* IEE, 93, (Part 3,21).

Kajfez D., *Influence of an airgap on the measurement of dielectric constants by a parallel-plate dielectric resonator,* IEE Proceedings Part H, v 133, n 4, (Aug 1986).

Katz H.W., ed, *Solid State Magnetic and Dielectric Devices,* USA: John Wiley and Sons, 1959.

Keller G.V., *Supplementary guide to the literature on Electrical properties of rocks and minerals.*

Krazewski A., *Microwave aquametry-A bibliography for 1955-1979,* Journal of Microwave Power, v 15, n 4, (1980).

Kumar A. and Smith G., *Microwave properties of yarns and textiles using a resonant microwave cavity,* IEEE Transactions IM-26, (1977).

Lakshminarayana M.R. et al, *Simple microwave technique for independent measurement of sample size and dielectric constant,* IEEE Transactions, MTT-27, (1979).

Liao S.Y., *Microwave Circuit Analysis and Amplifier Design,* New Jersey: Prentice-Hall, 1987.

Lyttle R.J., *Measurement of earth medium electrical characteristics: techniques and applications,* IEEE Transmissions on Geo Science Electron, vol 12, no 3, (1974).

Magerl G., *Novel method for cavity parameter measurement,* IEEE Trans Instrum Meas, v IM-25, n 2, (Jun 1976).

Mehdizadeh M. et al, *Loop-gap resonator: A lumped mode microwave resonant structure,* IEEE Transactions on microwave theory and techniques, vol 31, (1983).

Mercer S., *On-line Microwave measurement of complex dielectric constant,* PhD Thesis, Department of Electrical and Electronic Engineering, UCT, 1990.

Mercer S., *Rock Differentiation using Microwave irradiation,* MSc Thesis, Department of Electrical and Electronic Engineering, UCT, 1987.

Montgomery C., *Techniques of Microwave Measurement,* M.I.T. Radiation laboratory series, USA: McGraw-Hill, 1947.

Parkhomenko E.I., *Electrical Properties of rocks,* New York: Plenum Press, 1967.

Pozar D.M., *Microwave Engineering,* USA: Addison-Wesley Publishing company, 1990.

Radebe K. G., *Investigation of transmission line resonant structures and development of associated measuring techniques for rock sorting,* Unpublished 4th year Thesis, Department of Electrical and Electronic Engineering, UCT, 1988.

Ramo S. and Whinnery J. R., *Fields and waves in modern Radio,* USA: John Wiley and Sons, 1947.

Ramo S. et al, *Fields and waves in communication electronics,* 2nd ed, USA: John Wiley and Sons, 1967.

Roberts J., *Dielectric response of material media using the detuning of a resonant microwave cavity,* Microwave Power Electromagn, v 22, n 3, (1987).

Rose R.M. et al, *Electronic properties, vol IV, The structure and properties of materials,* USA: John Wiley and Sons, 1966.

Sanchez M.C., *Automatic technique for the characterization of a dielectric resonator coupled to a microstrip line,* IEE Proceedings Part H, v 133, n 2, (Apr 1986), p99-102.

Smyth C.P., *Dielectric Behaviour and Structure,* International Chemical Series, USA: McGraw-Hill, 1955.

South Africa 1988-1989, Official yearbook of the Republic of South Africa, Ed. Bureau of Information, Cape Town: CTP Printers, 1989.

Tanabe E. and Joines W. T., *A non-destructive method for measuring the complex permittivity of dielectric materials at microwave frequencies using an open transmission line resonator,* IEEE Transactions on Instrum. Meas., vol IM-25, (1976).

Webb W. E. and Church R. H., *Measurement of dielectric properties of minerals at microwave frequencies,*

Zheng W., *Complex resonant frequencies of open composite dielectric resonators,* European Microwave conference : Microwave 87, Rome, Italy, Published by Microwave Exhibitions and Publications, Turnbridge Well, England, (1987).

APPENDIX I

EVALUATION OF THE RESONANT FREQUENCY OF A CAVITY

If the waveguide region is source-free, Maxwell's equations can be written as:

$$\nabla \times \mathbf{E} = -j\omega\mu\mathbf{H} \qquad 1a$$

$$\nabla \times \mathbf{H} = j\omega\epsilon\mathbf{E} \qquad 1b$$

with an $e^{-j\beta z}z$ dependence, the three components of each of the above vector equations can be written as:

$$\frac{\partial E_z}{\partial y} + j\beta E_y = -j\omega\mu H_x \qquad 2a$$

$$-j\beta E_x - \frac{\partial E_z}{\partial x} = -j\omega\mu H_y \qquad 2b$$

$$\frac{\partial E_y}{\partial x} - \frac{\partial E_x}{\partial y} = -j\omega\mu H_z \qquad 2c$$

$$\frac{\partial H_z}{\partial y} + j\beta H_y = j\omega\epsilon E_x \qquad 3a$$

$$-j\beta H_x - \frac{\partial H_z}{\partial x} = j\omega\epsilon E_y \qquad 3b$$

$$\frac{\partial H_y}{\partial x} - \frac{\partial H_x}{\partial y} = j\omega\epsilon E_z \qquad 3c$$

The above equations can be solved for the four transverse field components in terms of E_z and H_z to give:

$$H_x = \frac{j}{k_c^2}\left(\omega\epsilon\frac{\partial E_z}{\partial y} - \beta\frac{\partial H_z}{\partial x}\right) \qquad 4a$$

$$H_y = -\frac{j}{k_c^2}\left(\omega\epsilon\frac{\partial E_z}{\partial x} + \beta\frac{\partial H_z}{\partial y}\right) \qquad 4b$$

$$E_x = -\frac{j}{k_c^2}\left(\beta\frac{\partial E_z}{\partial x} + \omega\mu\frac{\partial H_z}{\partial y}\right) \qquad 4c$$

$$E_y = \frac{j}{k_c^2}\left(-\beta\frac{\partial E_z}{\partial y} + \omega\mu\frac{\partial H_z}{\partial x}\right) \qquad 4d$$

where $k_c^2 = k^2 - \beta^2$ and is called the cut-off wave number and

$$k = \omega\sqrt{\mu\epsilon} = \frac{2\pi}{\lambda}$$

For TE waves, $E_z = 0$, $H_z \neq 0$. Equations 4 then reduce to:

$$H_x = \frac{-j\beta}{k_c^2}\frac{\partial H_z}{\partial x} \qquad 5a$$

$$H_y = \frac{-j\beta}{k_c^2}\frac{\partial H_z}{\partial y} \qquad 5b$$

$$E_x = \frac{-j\omega\mu}{k_c^2}\frac{\partial H_z}{\partial y} \qquad 5c$$

$$E_y = \frac{j\omega\mu}{k_c^2}\frac{\partial H_z}{\partial x} \qquad 5d$$

In this case $k_c \neq 0$, $\beta = \sqrt{k^2 - k_c^2}$ is called the propagation constant.

Since $H_z(x, y, z) = h_z(x, y)e^{-j\beta z}$, the Helmholtz wave equation:

$$\left(\frac{\partial^2}{\partial x^2} + \frac{\partial^2}{\partial y^2} + \frac{\partial^2}{\partial z^2} + k^2\right)H_z = 0 \qquad 6$$

reduces to a 2-D wave equation for h_z as shown below.

$$\left(\frac{\partial^2}{\partial x^2}+\frac{\partial^2}{\partial y^2}+k_c^2\right)h_z(x,y)=0 \qquad 7$$

since $k_c^2 = k^2 - \beta^2$

Using the method of separation of variables to solve 7 we obtain:

$$\frac{1}{X}\frac{d^2X}{dx^2}+\frac{1}{Y}\frac{d^2Y}{dy^2}+k_c^2=0 \qquad 8$$

where $h_z(x,y)=X(x)Y(y)$

Each of the terms of equation 8 must be equal to a constant. Defining separation constants k_x and k_y we obtain:

$$\frac{d^2X}{dx^2}+k_x^2X=0 \qquad 9a$$

$$\frac{d^2Y}{dy^2}+k_y^2Y=0 \qquad 9b$$

$$k_x^2+k_y^2=k_c^2 \qquad 9c$$

The general solution for $h_z(x,y)$ can be written as:

$$h_z(x,y)=(A\cos k_x x+B\sin k_x x)(C\cos k_y y+D\sin k_y y) \qquad 10$$

Applying the boundary conditions we find that:

$$D=0,\quad k_y=\frac{n\pi}{b},\quad B=0,\quad k_x=\frac{m\pi}{a}$$

for n,m=0,1,2,... . $H_z(x,y,z)$ is then:

$$H_z(x,y,z)=A_{mn}\cos\frac{m\pi x}{a}\cos\frac{n\pi y}{b}e^{-j\beta z} \qquad 11$$

where A_{mn} is an arbitrary amplitude constant composed of A and C.

Substituting equation 11 into equation 4 the transverse field components of the TE_{mn} mode can then be found. They are:

$$E_x = \frac{j\omega\mu n\pi}{k_c^2 b} A_{mn} \cos\frac{m\pi x}{a} \sin\frac{n\pi y}{b} e^{-j\beta z} \qquad 12a$$

$$E_y = \frac{-j\omega\mu m\pi}{k_c^2 a} A_{mn} \sin\frac{m\pi x}{a} \cos\frac{n\pi y}{b} e^{-j\beta z} \qquad 12b$$

$$H_x = \frac{j\beta m\pi}{k_c^2 a} A_{mn} \sin\frac{m\pi x}{a} \cos\frac{n\pi y}{b} e^{-j\beta z} \qquad 12c$$

$$H_y = \frac{j\beta n\pi}{k_c^2 b} A_{mn} \cos\frac{m\pi x}{a} \sin\frac{n\pi y}{b} e^{-j\beta z} \qquad 12d$$

The propagation constant is:

$$\beta = \sqrt{k^2 = k_c^2} = \sqrt{k^2 - \left(\frac{m\pi}{a}\right)^2 - \left(\frac{n\pi}{b}\right)^2} \qquad 12e$$

Each mode thus has a cut-off frequency f_{cmn} given by:

$$f_{cmn} = \frac{k_{cmn}}{2\pi\sqrt{\mu\epsilon}} = \frac{1}{2\pi\sqrt{\mu\epsilon}} \sqrt{\left(\frac{m\pi}{a}\right)^2 + \left(\frac{n\pi}{b}\right)^2} \qquad 13$$

where k_{cmn} is the cut-off wave number.

For a rectangular resonant cavity, the cut-off wave number becomes:

$$k_{cmnl} = \sqrt{\left(\frac{m\pi}{a}\right)^2 + \left(\frac{n\pi}{b}\right)^2 + \left(\frac{l\pi}{d}\right)^2} \qquad 14$$

and the cut-off frequency becomes:

$$f_{cmnl} = \frac{c}{2\pi\sqrt{\mu_r\epsilon_r}} \sqrt{\left(\frac{m\pi}{a}\right)^2 + \left(\frac{n\pi}{b}\right)^2 + \left(\frac{l\pi}{d}\right)^2} \qquad 15$$

APPENDIX II

CHOICE OF CAVITY DIMENSIONS AND SIDES ON WHICH TO CUT SLOTS

Cavity dimensions

From equation 12e in Appendix I, non-trivial solutions of Maxwell's equations will only exist for

$\beta_{mnl} = l\pi \quad where \quad l = 1, 2, 3, \ldots$

This implies that the cavity must be an integer multiple of a half-guide wavelength long at the resonant frequency.

Therefore the cut-off wave number for the rectangular cavity can be defined as:

$$k_{mnl} = \sqrt{\left(\frac{m\pi}{a}\right)^2 + \left(\frac{n\pi}{b}\right)^2 + \left(\frac{l\pi}{d}\right)^2} \qquad 1$$

But $k = 2\pi/\lambda$. From the basic relation $\lambda = c/f$, $k = 2\pi f/c$.

The resonant frequency of the TE_{mnl} or TM_{mnl} mode with air as dielectric is given by:

$$f_{mnl} = \frac{k_{mnl}c}{2\pi} = \frac{c}{2\pi}\sqrt{\left(\frac{m\pi}{a}\right)^2 + \left(\frac{n\pi}{b}\right)^2 + \left(\frac{l\pi}{d}\right)^2} \qquad 2$$

For the TE_{101} mode, m=l=1 and n=0.

$$\therefore \quad f_{101} = \frac{c}{2\pi}\sqrt{\left(\frac{\pi}{a}\right)^2 + \left(\frac{\pi}{d}\right)^2} \qquad 3$$

Enforcing the waveguide criterion that $\lambda_0 > a > \lambda_0/2$ where λ_0 is the free-space wavelength and is equal to 0.6m for a resonant frequency of 500MHz; we obtain a=0.450m. Substituting this into equation 3 we obtain d=0.403m. The remaining dimension,b is chosen as half of a i.e. b=0.225m.

Cutting of slots

A way of introducing the samples into and retrieving them from the resonant cavity is required. This is done via two slots cut on parallel sides of the cavity. The choice of the two sides should be made in such a way as to ensure minimum radiation out of the cavity. At this point it would be instructive to try and explain the radiation mechanism.

Figure 1 below shows the cavity with the magnetic field lines and direction of flow of the surface current.

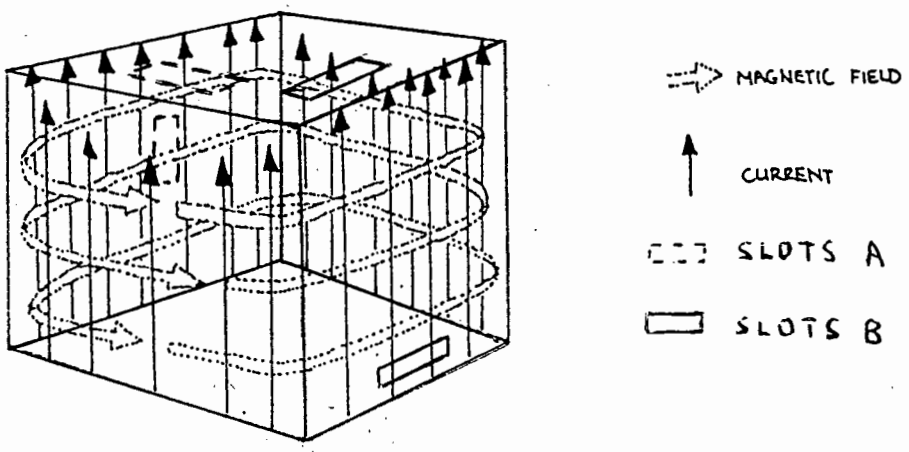

Fig.1 Resonant cavity showing H-field and current lines.

Radiating slots cut the direction of current flow. Therefore slots A would be non-radiating slots; even though slight radiation still exists out of these slots. Slots B would be radiating slots.

APPENDIX III

COMPUTER PROGRAM TO PROCESS DYNAMIC TESTS DATA

A computer program that was used to process data from the dynamic tests is given on the next page. This program was written in Pascal by personnel at the De Beers Research Laboratory in Johannesburg.

```
PROGRAM Mag_res;

$I a:typedef.sys}
$I a:graphix.sys}
$I a:kernel.sys}

 CONST
    max_buffer        = 3000;
    Trigger           = 0;
    Frequency_shift   = 1;
    Amplitude_change = 2;


 TYPE
   time_string = string[11];

 VAR

   TimeStart, TimeEnd : Time_string;
   Testing,
   SaveIt           : boolean;
   Test_array       : array [Frequency_shift..Amplitude_change,1..Max_buffer]
   FileName         : string[8];
-------------------------------------------------------------------------------
 FUNCTION Time: Time_String;

    TYPE
      regpack = record
                  ax,bx,cx,dx,bp,si,di,ds,es,flags: integer;
                end;

   VAR
     recpack:           regpack;              {assign record}
     ah,al,ch,cl,dh:    byte;
     hour,min,sec,hun:      string[2];

   BEGIN
     ah := $2c;                               {initialize correct registers}
     with recpack do
     BEGIN
       ax := ah shl 8 + al;
     END;
     intr($21,recpack);                       {call interrupt}
     WITH recpack DO
     BEGIN
       str(cx shr 8,hour);                    {convert to string}
       str(cx mod 256,min);                         { " }
       str(dx shr 8,sec);                           { " }
       str(dx mod 256,hun);
     END;
     IF length(hour) = 1 THEN
       hour := '0' + hour;
     IF length(min) = 1 THEN
       min := '0' + min;
     IF length(sec) = 1 THEN
       sec := '0' + sec;
     IF length(hun) = 1 THEN
       hun := '0' + hun;
     time := hour+':'+min+':'+sec+'.'+hun;
   END;
-------------------------------------------------------------------------------
```

```
PROCEDURE FlushBuffer;

  TYPE
    RegPack   =  RECORD case Integer OF
                   1 : (ax,bx,cx,dx,bp,si,di,ds,es,flags : integer);
                   2 : (al,ah,bl,bh,cl,ch,dl,dh          : byte   );
                 END;

  VAR
    regs : regpack;

  BEGIN
    WITH regs DO
    BEGIN
      ah := $0C;
      al := 0;
      MsDos(Regs);
    END;
  END;
```

```
PROCEDURE Box(X1,Y1,X2,Y2 : integer);

  CONST
    TL = 'Ö';
    TR = 'Ç';
    BR = 'ì';
    BL = 'â';
    VL = '°';
    HL = 'á';

  VAR
    Horiz,
    Vert      : integer;

  BEGIN
    GoToXY(X1,Y1);
    Write(TL);
    FOR Horiz := (X1 + 1) TO (X2 - 1) DO
    BEGIN
      GoToXY(Horiz,Y1);
      Write(HL);
    END;
    GoToXY(X2,Y1);
    Write(TR);
    FOR Vert := (Y1 + 1) TO (Y2 - 1) DO
    BEGIN
      GoToXY(X2,Vert);
      Write(VL);
    END;
    GoToXY(X2,Y2);
    Write(BR);
    FOR Horiz := (X1 + 1) TO (X2 - 1) DO
    BEGIN
      GoToXY(Horiz,Y2);
      Write(HL);
    END;
    GoToXY(X1,Y2);
    Write(BL);
    FOR Vert := (Y1 + 1) TO (Y2 - 1) DO
    BEGIN
```

```
      GoToXY(X1,Vert);
      Write(VL);
    END;
  END;
{------------------------------------------------------------------------}
  FUNCTION AdSample(Chan : integer) : integer;

    VAR
      I : integer;

    BEGIN
      Port[$702] := 02;
      Port[$702] := chan * $10 + 3;
      FOR I := 1 TO 3 DO
        BEGIN
        END;
      AdSample := (Port[$701] AND $0F) * 256 + port[$700];
    END;

{------------------------------------------------------------------------}
FUNCTION YesNo : char;

  VAR
    TempChar : char;

  BEGIN
    REPEAT
      REPEAT UNTIL KeyPressed;
      IF KeyPressed THEN
        Read(Kbd,TempChar);
      TempChar := UpCase(TempChar);
    UNTIL ((TempChar = 'Y') OR (TempChar = 'N'));
    YesNo := TempChar;
  END;
{------------------------------------------------------------------------}
PROCEDURE GetMin( VAR Min_Amp,Min_Freq : REAL; VAR Pos_in_array : INTEGER);

  VAR
      Countmm : integer;

  BEGIN
    Min_Amp  := 9999;
    Min_Freq := 9999;
    FOR Countmm := 1 TO Max_buffer DO
      BEGIN
        IF Test_array[Frequency_shift,Countmm] < Min_Freq THEN
          BEGIN
            Min_Freq := Test_array[Frequency_shift,Countmm];
            Pos_in_array:= Countmm;
          END;
        IF Test_array[Amplitude_change,Countmm] < Min_Amp THEN
          Min_Amp := Test_array[Amplitude_change,Countmm];
      END;
      Min_Amp  := Min_Amp * 10 / 4095;
      Min_Freq := Min_Freq * 10 / 4095;
  END;

{------------------------------------------------------------------------}
PROCEDURE DrawGraph;

  VAR
    MinPos,
    OldX,
```

```
  OldY,
  Xpos,
  Ypos,
  CountDGA,
  Range,
  Posinarray,
  CountDG : integer;
  Temp_amp,Temp,
  Temp_freq   : real;
  DrawIt,
  KeyIn   : char;
  Min     : Integer;
  First,Last,X,Count : Integer;
  T_array            : ARRAY [Frequency_shift..Amplitude_change,1..1001]

BEGIN
    EnterGraphic;
    DefineWorld(1,0,0,639,199);
    SelectWorld(1);
    SelectWindow(1);
    DrawLine(39,20,639,20);
    DrawLine(38,180,38,20);
    DrawLine(37,180,37,20);
    FOR CountDG := 1 TO 5 DO
      DrawLine(30,(Countdg)*32+20,38,(CountDG)*32+20);
    FOR CountDG := 0 TO 2 DO
    BEGIN
      Xpos := 300 * CountDG  + 39;
      IF Xpos < 0 THEN Xpos := 0;
      DrawLine(Xpos,10,Xpos,20);
    END;

    OldX := 39;
    OldY := 20;
   {.....................................}

    GetMin(Temp_amp,Temp_freq,MinPos);
    First := (MinPos - 500);
    IF First <= 0 THEN
       First := 1;
    Last  := MinPos + 500;
    IF Last > Max_buffer THEN
       Last := Max_buffer;

    Range := Last - First;
    X := 0;
    FOR Count:=First TO Last DO
      BEGIN
        X := X + 1;
        T_array [Amplitude_change,x] := Test_array [Amplitude_change,Coun
        T_array [Frequency_shift,x] := Test_array [Frequency_shift,Count]
      END;
    {.....................................}

    FOR CountDG := 39 TO 639 DO
    BEGIN
      PosInArray := Trunc((CountDG-39) * (Range / 600) + 1);

      Temp := T_array[Frequency_shift,PosInArray];
      Temp := (Temp * 160 / 2048);
      YPos := Trunc(Temp);
      XPos := CountDG;

      DrawLine(OldX,OldY,XPos,YPos);
```

```
        OldY := YPos;
        OldX := XPos;
      END;
      OldX := 39;
      OldY := 20;
      FOR CountDG := 39 TO 639 DO
      BEGIN
        PosInArray := Trunc((CountDG-39) * (Range / 600) + 1);

        Temp := T_array[Amplitude_change,PosInArray];
        Temp := (Temp * 160 / 2048);
        YPos := Trunc(Temp);
        XPos := CountDG;

        DrawLine(OldX,OldY,XPos,YPos);

        OldY := YPos;
        OldX := XPos;
      END;
      FlushBuffer;
      Sound(400);
      Delay(100);
      NoSound;

      GoToXY(25,25);

      DrawText(300,330,2,'Save this? (Y/N) - ');
      FlushBuffer;
      KeyIn := YesNo;
      SaveIt := (KeyIn = 'Y');

      LeaveGraphic;
  END;
-------------------------------------------------------------------------------
PROCEDURE Start;

  VAR
    Sp_bar_pressed : boolean;
    Key            : char;

  BEGIN
    ClrScr;
    Box(20,5,60,7);
    GoToXY(28,6); Write('Gabbro or kimberlite? (G/K)');
    Flushbuffer;
    REPEAT
      Read(Kbd,Key);
      Key := UpCase(Key);
    UNTIL ((Key = 'G') OR (Key = 'K'));
    IF Key = 'G' THEN
      FileName := 'GABBRO'
    ELSE
      FileName := 'KIMBERLI';
    ClrScr;
    Sound (400); Delay (100); Sound (800); Delay (200); NoSound;
  END;
-------------------------------------------------------------------------------
PROCEDURE RunTest;

VAR
  chan,
```

```
  I,
  counter          : integer;

BEGIN
  REPEAT
    Delay(1);
  UNTIL Adsample(Trigger) < 200;
  TimeStart := Time;
  FOR counter := 1 TO Max_buffer DO
    BEGIN
        Port[$702] := 02;
        Port[$702] := Amplitude_Change * $10 + 3;
        FOR I := 1 TO 3 DO
          BEGIN
          END;
        Test_array [Amplitude_change,counter] := (Port[$701] AND $0F) * 256

        Port[$702] := 02;
        Port[$702] := Frequency_shift * $10 + 3;
        FOR I := 1 TO 3 DO
          BEGIN
          END;
        Test_array [Frequency_shift,counter] := (Port[$701] AND $0F) * 256
    END;
  TimeEnd := Time;
  FlushBuffer;
END;


{-------------------------------------------------------------------------}
PROCEDURE Store_data;

VAR
     FileOut      : TEXT;
     First,Last,
     Countsave    : INTEGER;
     Percent,
     VoltsF,
     VoltsA       : REAL;
     MinA,MinF    : Real;
     Pos_in_array : Integer;

BEGIN
  ClrScr;
  GoToXY(31,12);
  Write('- STORING DATA! -');
  GetMin (MinA,MinF,Pos_in_array);
  Assign(Fileout,FileName + '.PRN');
  {$I-}
  Append(Fileout);
  {$I+}
  IF IOResult = 0 THEN
    WriteLn(FileOut,MinA:4:2,MinF:5:2)
  ELSE
  BEGIN
    ReWrite(FileOut);
    WriteLn(FileOut,'"Amplitude","Frequency"');
    WriteLn(FileOut,MinA:4:2,MinF:5:2);
  END;
  Close(Fileout);
END;

{-------------------------------------------------------------------------}
PROCEDURE RunSeries;
```

```
  VAR
    TestNo          : char;
    Rock_name       : string[8];

  BEGIN
      SaveIt := False;
      REPEAT
        ClrScr;
        Box(27,8,52,10);
        GoToXY(29,9); Write('- WAITING FOR SAMPLE -');
        RunTest;
        DrawGraph;
      UNTIL SaveIt;
      Store_Data;
  END;
```

```
BEGIN
  Port[$703] := $92;
  Testing := True;
  InitGraphic;
  LeaveGraphic;
  WHILE Testing DO
  BEGIN
    Start;
    RunSeries;
    ClrScr;
    Box(32,11,47,13);
    GoToXY(34,12);
    Write('Quit? (Y/N)');
    FlushBuffer;
    Testing := ('N' = YesNo);
  END;
  ClrScr;
END.
```